Huang *et al. Chem. Synth.* **2025**, *5*, 57
DOI: 10.20517/cs.2024.142

Chemical Synthesis

Review

Open Access

Corrosion engineering for electrode fabrication toward alkaline water electrolysis

Quanbin Huang[1], Xu Zhang[1], Shiwei Lin[1], Yipu Liu[1,*], Xiaoxin Zou[2], Hui Chen[2,*]

[1]School of Materials Science and Engineering, Key Laboratory of Pico Electron Microscopy of Hainan Province, Hainan University, Haikou 570228, Hainan, China.
[2]State Key Laboratory of Inorganic Synthesis and Preparative Chemistry, College of Chemistry, Jilin University, Changchun 130012, Jilin, China.

[*]**Correspondence to:** Prof. Hui Chen, State Key Laboratory of Inorganic Synthesis and Preparative Chemistry, College of Chemistry, Jilin University, 2699 Qianjin Street, Changchun 130012, Jilin, China. E-mail: chenhui@jlu.edu.cn; Prof. Yipu Liu, School of Materials Science and Engineering, Key Laboratory of Pico Electron Microscopy of Hainan Province, Hainan University, 58 Renmin Avenue, Haikou 570228, Hainan, China. E-mail: liuyp@hainanu.edu.cn

How to cite this article: Huang, Q.; Zhang, X.; Lin, S.; Liu, Y.; Zou, X.; Chen, H. Corrosion engineering for electrode fabrication toward alkaline water electrolysis. *Chem. Synth.* **2025**, *5*, 57. https://dx.doi.org/10.20517/cs.2024.142

Received: 2 Oct 2024 **First Decision:** 23 Oct 2024 **Revised:** 6 Dec 2024 **Accepted:** 9 Dec 2024 **Published:** 20 Jun 2025

Academic Editor: Xiang-Dong Yao **Copy Editor:** Pei-Yun Wang **Production Editor:** Pei-Yun Wang

Abstract

Alkaline water electrolysis is a promising technology for producing green hydrogen at scale. The electrodes are the heart of an alkaline water electrolyzer, directly determining its performance and durability. In recent years, corrosion engineering has emerged as a powerful strategy to enable next-generation efficient electrodes for industrial use, thanks to its low cost, ease of scale-up and simple operation. This review highlights recent groundbreaking studies in corrosion engineering for electrode fabrication, mainly including oxygen corrosion, hydrogen evolution corrosion, oxidant corrosion, and microbial corrosion. We introduce the mechanisms of these four corrosion reactions, along with effective strategies for accelerating the processes and modifying the corrosion products. Finally, we propose future prospects of corrosion techniques in industrial hydrogen production.

Keywords: Corrosion engineering, electrocatalysis, electrode, alkaline water electrolysis, green hydrogen

INTRODUCTION

With the global energy crisis worsening, hydrogen is gaining more attention as a clean energy carrier[1-3]. Water electrolysis is an important technological pathway for industrial green hydrogen production[4].

However, to make it viable on an industrial scale, energy conversion efficiency must be improved to lower the cost of green hydrogen[5]. The alkaline water electrolyzer has developed since the 1920s into a mature and cost-effective technology, suitable for large-scale hydrogen production in industrial settings[6]. Nickel meshes and Raney nickel electrodes are the primary electrode materials used in commercial alkaline water electrolyzers[7]. In industrial water electrolysis settings (6 M KOH, ≥ 60 °C, ≥ 1 $A \cdot cm^{-2}$), the electrode should maintain high hydrogen production efficiency at high current densities, which imposes higher demands on both the activity and stability of the electrodes[8-10]. Meanwhile, the negative impacts of bubble adhesion and electrolyte corrosion on the electrodes should not be overlooked[11]. The active material on the electrode is prone to detachment due to these factors during prolonged operation, which leads to performance degradation[12]. In response to these challenges, numerous electrode materials with high activity and stability have been synthesized at the research level[13-15]. However, the involved synthesis strategies (such as high-temperature calcination[16,17], hydrothermal methods[18,19], *etc.*) are difficult to scale up for producing large-area electrodes compatible with industrial electrolyzers[20]. Consequently, developing low-cost, scalable electrode materials with high activity and durability is crucial for advancing the industrial application of water electrolysis.

Corrosion engineering, which primarily involves regulating the corrosion reaction to promote the growth of beneficial corrosion products on the metal substrate, has been confirmed to successfully synthesize a series of highly active oxygen evolution reaction (OER) catalysts[21-23], which serves as the bottleneck in water electrolysis due to the four-electron process. As early as 2016, Zhang *et al.* applied corrosion engineering for the preparation of OER catalysts[24]. Subsequently, in 2018, Liu *et al.* synthesized large-area NiFe layered double hydroxide (NiFe-LDH) catalysts through iron-based oxygen corrosion, showing more than 6,000 h of OER stability in alkaline electrolytes[25]. Since then, numerous high-performance materials synthesized by corrosion methods have been reported[26-28]. Some novel corrosion methods, such as microbial corrosion, have also been developed. By 2022, Zhao *et al.* further advanced the understanding of the corrosion mechanism based on the work of Zou[29]. With the in-depth research into corrosion engineering, its potential applications in the preparation of OER catalysts have become increasingly evident[30]. Moreover, compared with high-temperature calcination, hydrothermal methods and other synthesis strategies, corrosion engineering is simple to operate, with easily controllable process conditions, allowing for high reproducibility in large-scale production. Therefore, it holds broad application potential in the preparation of OER catalysts under industrial conditions.

In this review, we primarily present corrosion-based methods from an industrial perspective, categorizing them into four types based on corrosion mechanisms: oxygen corrosion, hydrogen evolution corrosion, oxidant corrosion and microbial corrosion [Figure 1A-D]. We highlight the latest advances in corrosion engineering for promising catalysts, covering aspects such as structural design, controllable synthesis, mechanistic exploration, and performance optimization. Additionally, we assess the scalability of these methods and finally offer perspectives on the application of corrosion techniques in industrial hydrogen production.

OXYGEN CORROSION

Oxygen corrosion is an electrochemical corrosion caused by the reduction reaction of neutral oxygen molecules (O_2) at the cathode in a solution[31-33]. Its spontaneity depends on the electrode potential difference between the metal and oxygen[30]. Oxygen corrosion can happen spontaneously if the electrode potential of oxygen exceeds that of the metal. Throughout the oxygen corrosion process, a lower potential is exhibited at the metal surface, while a higher potential is associated with oxygen. This potential gradient triggers the transfer of electrons, resulting in the oxidation of metal atoms to form metal ions, while oxygen is reduced

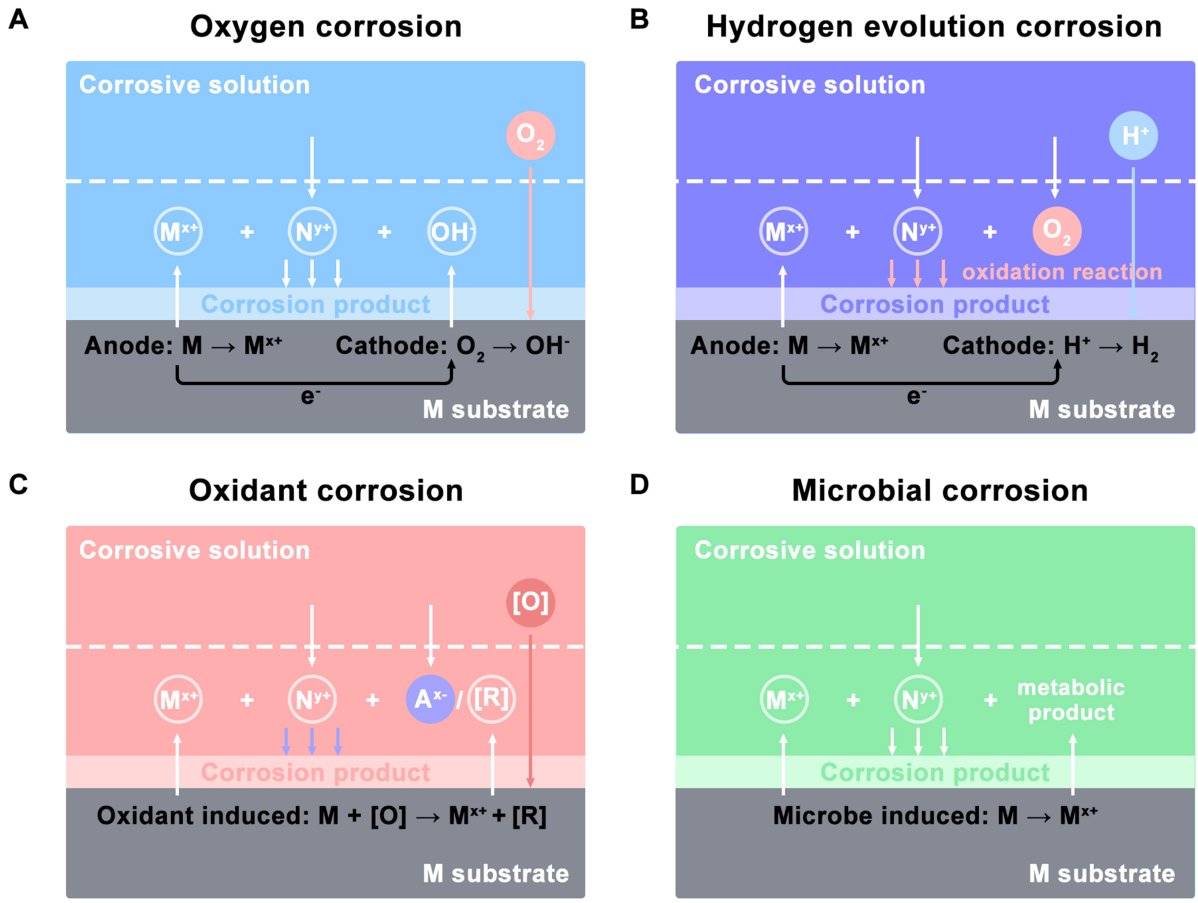

Figure 1. Four typical corrosion methods for electrode fabrication. (A) Oxygen corrosion; (B) Hydrogen evolution corrosion; (C) Oxidant corrosion; (D) Microbial corrosion. M represents the metal substrate, N^{y+} is other metal ions in corrosion solution, [O] denotes the oxidizing agent, [R] is the reduction product of the oxidant, and A^{x-} is the involved anions in corrosion solution.

to form hydroxide ions[30]. Subsequently, the metal ions can grow corrosion products on the metal surface due to localized pH elevation[34]. Here, we will first introduce the corrosion mechanisms of oxygen corrosion based on different types of substrates, and then explore effective methods for accelerating the corrosion process and further modifying the corrosion products.

Iron-based substrates are a type of substrate prone to oxygen corrosion, making corrosion engineering relatively easy to achieve[35]. Liu *et al.* synthesized a range of large-area iron-containing layered hydroxides by immersing iron plates in an aqueous solution of divalent cations [Figure 2A][25]. Among them, O_2-Cat-1, prepared using $NiSO_4$ solution, exhibited the highest OER catalytic activity. In 1 M KOH solution, an overpotential of only 257 mV was required to achieve a current density of 500 mA·cm^{-2}. Furthermore, it demonstrated significant catalytic stability for over 5,000 h at a high current density of 1,000 mA·cm^{-2}, indicating substantial potential for large-scale commercial water splitting technology [Figure 2B]. In the investigation of the oriented growth of LDH nanosheet arrays, Liu *et al.* cited the corrosion of iron substrates in $NiSO_4$ as an example, arguing that the classic heterogeneous nucleation/growth mechanism[36] provided a plausible explanation for the LDH growth process in corrosion engineering[25]. The driving force behind iron corrosion is regarded as the potential difference between Fe/Fe^{2+} and OH^-/O_2, which produces a considerable amount of iron ions and OH^- near the iron plate surface[33]. As the local pH increases, iron ions and OH^- co-precipitate with M^{2+} ions (M = Ni, Co, Mn, Mg) from the solution, resulting in the synthesis of

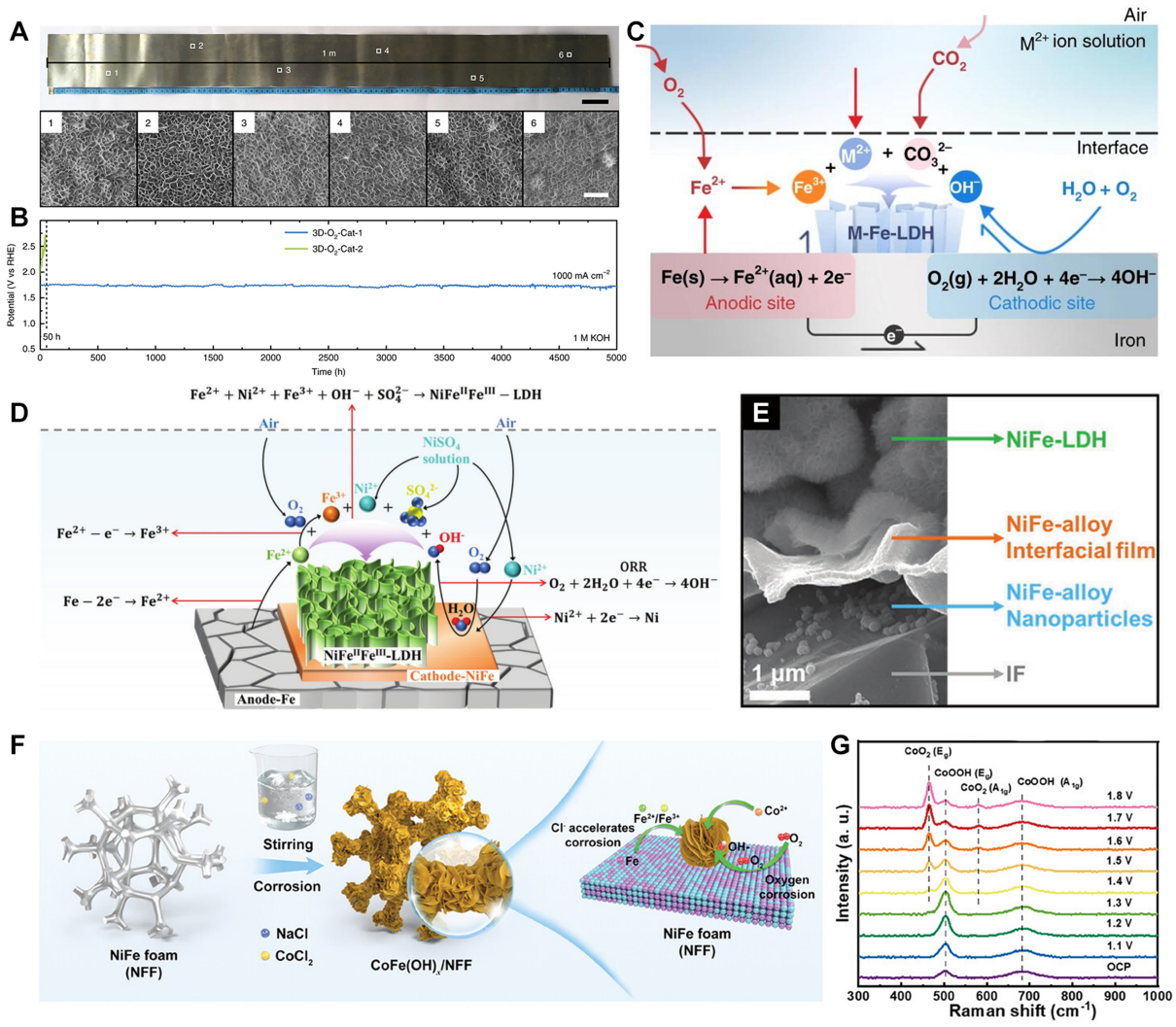

Figure 2. (A) Digital image of the electrode (0.1 × 1 m^2) and SEM images of the selected areas 1-6; (B) Chronopotentiometric curves of 3D-O_2-Cat-1 and 3D-O_2-Cat-2 in 1 M KOH at 1,000 mA·cm^{-2}; (C) Proposed corrosion mechanism for corrosion engineering[25]. Reproduced under the terms of the Creative Commons Attribution License; (D) Schematic of the NiFe-LDH@IF growth mechanism; (E) SEM image of the four-layer structure of NiFe-LDH@IF-200-72. Reproduced with permission[29]. Copyright 2021 Wiley-VCH; (F) Schematic of $CoFe(OH)_x$-m/NFF electrodes fabrication; (G) *In situ* Raman spectra of $CoFe(OH)_x$-500/NFF at different voltages during OER. Reproduced with permission[37]. Copyright 2024, Wiley-VCH. SEM: Scanning electron microscope; LDH: layered double hydroxide; IF: iron foam; OER: oxygen evolution reaction.

LDH on the iron substrate [Figure 2C]. Due to the anisotropic crystal structure of LDHs, growth along the ab direction occurs faster than along the c direction, leading to preferential growth of all nanosheets along the direction parallel to the corresponding basal planes[36].

Within the framework of this corrosion system, Zhao *et al.* conducted systematic investigations, asserting that the substitution reactions driven by differences in metal reactivity played a crucial role in the corrosion process[29]. Taking the corrosion of iron foam (IF) in Ni^{2+} solution as an example, the oxygen corrosion mechanism was further discussed and improved upon [Figure 2D]. The author believed that during corrosion, the Ni-Fe replacement reaction (1) occurs, resulting in the formation of a NiFe alloy on the IF. Due to the higher corrosion potential of the NiFe alloy compared to iron, it acts as the cathode and forms a corrosion cell with the IF. The IF anode loses electrons and releases Fe^{2+} (2). Some Fe^{2+} will be oxidized to

Fe^{3+} by the action of dissolved oxygen (3). Meanwhile, the oxygen reduction reaction (ORR, 4) is active at the NiFe alloy cathode surface. Within the alloy, the compact NiFe structure hinders Fe^{2+} diffusion outward, causing Fe^{2+} to accumulate and undergo hydrolysis, forming an acidic environment that facilitates hydrogen evolution reaction (HER, 5). The pH increase induced by HER and ORR encourages metal ion co-precipitation (Fe^{2+}, Fe^{3+}, Ni^{2+}), resulting in the formation of NiFe-LDH.

Replacement reaction:

$$Fe + Ni^{2+} \rightarrow Fe^{2+} + Ni \quad (1)$$

Oxidation reaction:

$$Fe - 2e^- \rightarrow Fe^{2+} \quad (2)$$

$$4Fe^{2+} + 2H_2O + O_2 \rightarrow 4Fe^{3+} + 4OH^- \quad (3)$$

Reduction reaction:

$$O_2 + 2H_2O + 4e^- \rightarrow 4OH^- \quad (4)$$

$$2H^+ + 2e^- \rightarrow H_2 \quad (5)$$

Precipitation reaction:

$$Fe^{2+} + Ni^{2+} + Fe^{3+} + OH^- + SO_4^{2-} \rightarrow NiFe^{II}Fe^{III}\text{-LDH} \quad (6)$$

As NiFe-LDH forms, the concentration of Ni^{2+} in the solution progressively decreases, resulting in the development of NiFe-LDH nanosheets characterized by a gradient of Ni^{2+} doping. After the consumption of Ni^{2+}, the residual Fe^{2+} and Fe^{3+} form iron hydroxides or hydroxide oxides on the top of nanosheets [Figure 2E]. Accordingly, the optimization of the electrocatalytic activity of NiFe-LDH@IF was achieved through the control of dissolved oxygen concentration by purging with N_2, as well as adjusting stirring, corrosion temperature, corrosion time, and solution concentration, affecting the quantities of α-FeOOH and NiFe-LDH and the doping level of Fe^{2+} in NiFe-LDH. The NiFe-LDH@IF-200-72 was synthesized, exhibiting a low Tafel slope (25.4 mV·dec^{-1}), low overpotential (η_{100} = 209 mV), excellent stability (100 mA·cm^{-2} for 192 h), and an approximately 100% Faradaic efficiency.

For the more complex corrosion behavior of NiFe alloys, Wang *et al.* proposed a passivation corrosion mechanism[37]. NiFe foam (NFF) was immersed in a solution containing NaCl and varying concentrations of $CoCl_2$, and stirred continuously at room temperature for 12 h, facilitating the growth of $CoFe(OH)_x$ nanosheets on the NFF [Figure 2F]. The authors indicated that in addition to the oxidation corrosion mechanism based on Liu's theory, transitions of Fe/Fe^{2+} and Fe^{2+}/Fe^{3+} occur at the anode, while ORR takes place at the cathode[25]. Subsequently, Co^{2+} from the solution co-precipitates to form $CoFe(OH)_x$. Moreover, considering the metal reactivity and the passivating effect of Co, a passivation corrosion mechanism is presented, as given in Equations (7) to (9). A substitution reaction between Co^{2+} and Fe occurs due to the potential difference between Co^{2+}/Co (-0.28 V) and Fe^{2+}/Fe (-0.44 V) (7). Given the passivating role of Co, a passivation reaction with O_2 is initiated (8), which subsequently interacts with Fe^{3+} in the presence of Cl^-,

leading to the formation of $CoFe(OH)_x$ (9). *In situ* Raman spectroscopy verifies the reconstruction of the electrode's surface structure and the formation of highly active Co(IV)-O sites during the OER process [Figure 2G]. The $CoFe(OH)_x$-500/NFF electrode exhibited excellent OER performance, demonstrating a very low overpotential (100 mA·cm^{-2}@274 mV) and rapid reaction kinetics (40.5 mV·dec^{-1}).

Replacement reaction:

$$Co^{2+} + Fe \rightarrow Co + Fe^{2+} \quad (7)$$

Passivation reaction:

$$Co + O_2 + 2H_2O \rightarrow CoO_xH_y \quad (8)$$

Depassivation reaction:

$$CoO_xH_y + Cl^- + Fe^{3+} + 2H_2O \rightarrow CoFe(OH)_x + Cl^- \quad (9)$$

The corrosion mechanisms of Ni substrates are subject to differing viewpoints. Lee *et al.* postulate, from a thermodynamic perspective, that in $Fe(NO_3)_3$ solution, Ni is oxidized by Fe^{3+} to form Ni^{2+}[38]. Zhang *et al.* analyze the corrosion current densities (I_{corr}) and corrosion potentials (E_{corr}) of NaCl (1.08 mA·cm^{-2}, -0.38 V), $Fe(NO_3)_3$ (3.06 mA·cm^{-2}, -0.18 V), and NaCl-$Fe(NO_3)_3$ (6.48 mA·cm^{-2}, -0.28 V), concluding that the Ni substrate has a propensity for self-corrosion in the NaCl-$FeNO_3$ solution, with Ni^{2+} dissolution being independent of Fe^{3+}[39]. As given in (10-12), rose-like NiFe-LDH is successfully synthesized. Ion exchange is then conducted to form a heterogeneous NiFe-LDH-Ni_3S_2 bifunctional electrode. The exceptional HER/OER performance is attributed to the heterogeneous structure of NiFe-LDH and Ni_3S_2, which enhances mass diffusion and reaction kinetics. The NiFe LDH-Ni_3S_2 electrode delivers 100 mA·cm^{-2} for both HER and OER in 1 M KOH seawater, with overpotential values of 257 and 280 mV, respectively.

Anode reaction:

$$Ni \rightarrow Ni^{2+} + 2e^-,\ Ni^{2+} \rightarrow Ni^{3+} + e^- \quad (10)$$

Cathode reaction:

$$O_2 + 2H_2O + 4e^- \rightarrow 4OH^- \quad (11)$$

Precipitation reaction:

$$Fe^{3+} + Ni^{2+} + Ni^{3+} + xOH^- \rightarrow NiFe(OH^-)_x \quad (12)$$

Through precise control of the oxygen corrosion environment, the corrosion process can be effectively modulated and accelerated[40,41]. For instance, an elevated concentration of Cl^- in the solution promotes metal ion dissolution, leading to an increased corrosion rate[39]. Meanwhile, the temperature of the corrosion environment can be increased to enhance the reaction between metal and oxygen[42]. Additionally, methods such as pH adjustment of the solution[43], optimization of metal concentration[44], addition of corrosion catalysts[45] and utilization of external polarization[46] are commonly implemented. These approaches not

only enhance synthesis efficiency but also enable the possibility of rapid corrosion in industrial applications.

By raising the concentration of Cl^- in the solution, the dissolution of metal ions can be facilitated, resulting in an increased corrosion rate[47]. In this regard, Li *et al.* achieved the successful preparation of nickel foam (NF)@NiFe-LDH-1.5-4 by soaking NF in a 1.5 M Cl^- solution for four minutes [Figure 3A][43]. The immersion of NF in NaCl, HCl, $Fe(NO_3)_3$, and $FeCl_3$ solutions revealed that Cl^- promoted the swift release of Ni^{2+}, and Fe^{3+} was beneficial for the formation of an open nanosheet architecture [Figure 3B]. The unique properties of Cl^- play a critical role in the removal of the metal passivation film. With a small ionic radius and strong penetration ability, Cl^- exhibits a high adsorption affinity for metal surfaces, which promotes their adsorption and accumulation on the passivation layer[47,48]. Some Cl^- ions are capable of traversing the passivation layer to access the metal surface. In this process, the passivation layer is compromised, and the diffusion of O_2 from the solution facilitates the release of metal surface atoms, resulting in the formation of soluble metal hydroxyl-chloride complexes [Figure 3C][39]. The NF@NiFe-LDH-1.5-4 exhibited exceptional OER performance in alkaline solution, requiring low overpotentials of 190 and 220 mV to achieve current densities of 100 and 657 mA·cm^{-2}, respectively. Additionally, the NF@NiFe-LDH-1.5-4 || NF@NiFe-LDH-1.5-4 electrolyzer operated stably for 320 h at a current density of 200 mA·cm^{-2} [Figure 3D].

In addition, Xia *et al.* reported a simple hydrothermal-assisted corrosion treatment method by increasing the corrosion temperature to accelerate the corrosion process[47]. The passivation layer of stainless steel is corroded by Cl^- under hydrothermal high-temperature conditions, leading to the dissolution of surface metal atoms. The OH^- provided by NaOH facilitates metal ion precipitation, forming a three-dimensional nanosheet array of the $NiFe_{1.833}(OH)_{0.5}O_{2.5}$ active catalytic layer. Density functional theory (DFT) calculations show that the formation of the $NiFe_{1.833}(OH)_{0.5}O_{2.5}$ active catalytic layer decreases the energy barrier of the rate-determining step and enhances the bonding between M and O^* intermediates, thus boosting OER performance. In 1 M KOH, the prepared electrode required an overpotential of 282 mV at 10 mA·cm^{-2}.

Based on the concept of corrosion engineering, other ions can be incorporated into the corrosion products to modify the intrinsic electronic structure, thereby optimizing the corresponding electrocatalytic performance[49,50]. Zhang *et al.* proposed a strategy utilizing oxidative corrosion engineering for synthesizing CoFe-LDH nanoflowers loaded with platinum nanoparticles (NPs)[51]. IF was immersed in a solution containing NaCl, $CoCl_2$, and H_2PtCl_6, and stirred for 15 h at room temperature to produce Pt-CoFe-LDH. Oxygen vacancy-rich CoFe-LDH nanoflowers are produced as NaCl accelerates the oxidative corrosion process, with platinum NPs self-assembling on the CoFe-LDH nanoflower surfaces. A three-dimensional nanoflower structure is characterized by a significant surface area and abundant exposed active sites, facilitating rapid mass transfer and ion diffusion. Furthermore, the presence of uniformly distributed Pt NPs promotes charge transfer and decreases the reaction barrier, resulting in improved performance for HER and OER. The overpotentials of Pt-CoFe-LDH electrodes reached as low as 126 mV for HER and 285 mV for OER at a current density of 100 mA·cm^{-2}. Simultaneously, the Pt-CoFe-LDH || Pt-CoFe-LDH electrolyzer demonstrated a small cell voltage of 1.66 V to achieve a current density of 50 mA·cm^{-2}, while maintaining excellent stability.

Catalysts synthesized through corrosion engineering are mostly oxides and (hydroxy)oxides[31], which serve as excellent precursor materials for the preparation of HER catalysts[39]. Zhang *et al.* reported a simple method for the large-scale modification of IF and its products[52]. The IF substrate was immersed in a 1 M $NiCl_2$ solution, resulting in the vertical growth of NiFe-O-nanowire arrays (NAs) on the surface of the IF [Figure 4A-C]. Experimental results and theoretical calculations indicate that trace iron doping significantly enhances the corrosion resistance of the active surface layer and decreases the reaction energy barrier for the

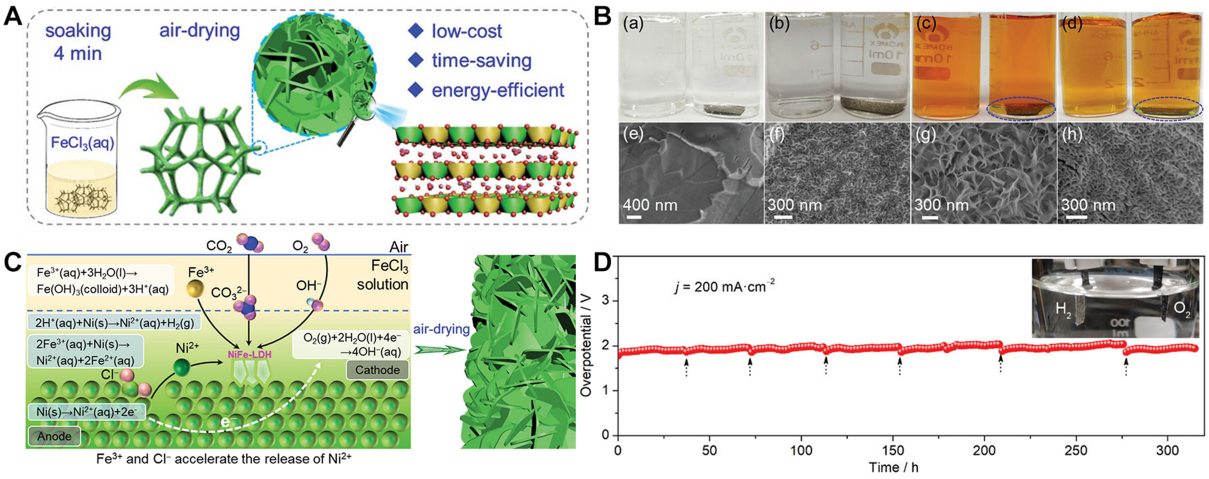

Figure 3. (A) Schematic for the synthesis of NF@NiFe-LDH-1.5-4; (B) The digital photographs and SEM images for different materials under various solutions; (C) The possible formation mechanism of NF@NiFe-LDH-1.5-4; (D) Chronopotentiometric curve at 200 mA·cm^{-2} for the NF@NiFe-LDH-1.5-4 || NF@NiFe-LDH-1.5-4 electrolytic cell. Reproduced with permission[43]. Copyright 2022 Wiley-VCH. NF: Nickel foam; LDH: layered double hydroxide; SEM: scanning electron microscope.

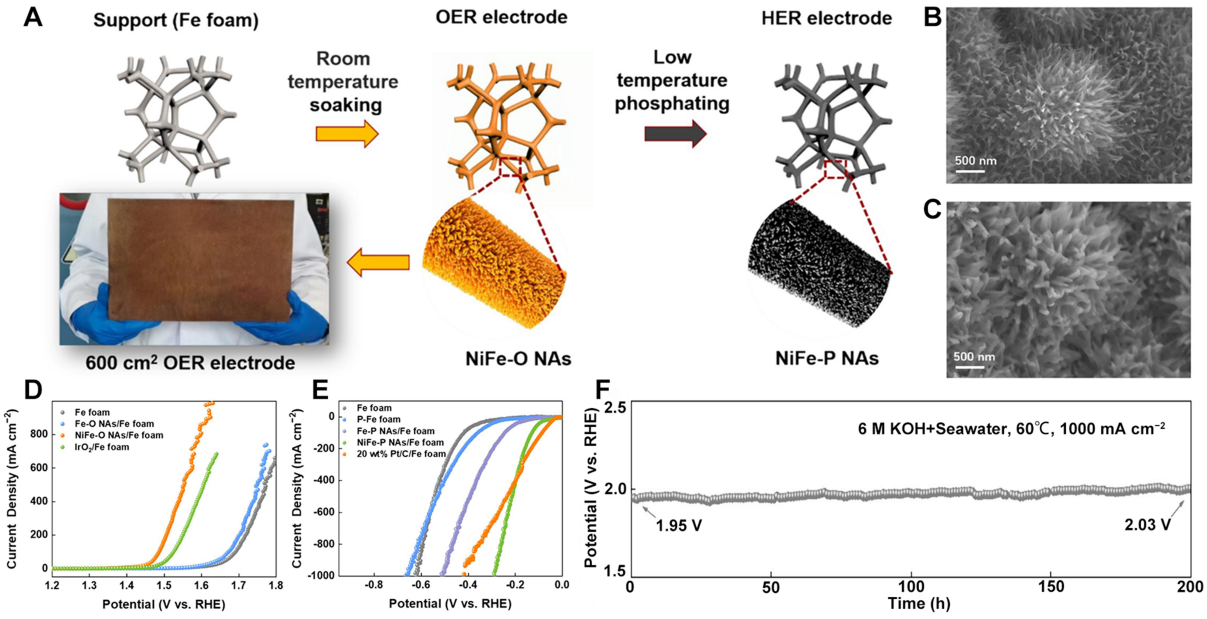

Figure 4. (A) Schematic of the synthesis procedures for the Fe foam supported NiFe-X NAs (X = O, P) and a 600 cm^2 OER electrode; (B) SEM images of NiFe-O NAs/Fe foam; (C) SEM images of NiFe-P nanowire; (D) OER polarization curves under 0-1,000 mA·cm^{-2} in 1 M KOH; (E) HER polarization curves under 0-1,000 mA·cm^{-2} in 1 M KOH; (F) Chronopotentiometric curves of the electrolyzer (6 M KOH + seawater, 60 °C, 1,000 mA·cm^{-2}). Reproduced with permission[52]. Copyright 2024, Elsevier. NAs: Nanowire arrays; OER: oxygen evolution reaction; SEM: scanning electron microscope; HER: hydrogen evolution reaction.

in situ formation of NiFeOOH active sites. The synthesized NiFe-O-NAs exhibited excellent OER performance, requiring overpotentials of 369 and 427 mV to achieve current densities of 500 and 1,000 mA·cm^{-2} in 1 M KOH freshwater, respectively [Figure 4D]. NiFe-P-NAs were formed by low-temperature phosphating of NiFe-O-NAs. The NiFe-P-NAs demonstrated superior HER performance, with overpotentials of 252 and 311 mV needed to attain current densities of 500 and 1,000 mA·cm^{-2} in 1 M KOH freshwater, respectively [Figure 4E]. NiFe-O-NAs and NiFe-P-NAs were integrated into an electrolyzer and

tested for stability over 200 h under simulated industrial conditions (6 M KOH, 60 °C, ≥ 1,000 $mA·cm^{-2}$), showing no significant degradation, thus confirming the excellent stability of both NiFe-O-NAs and NiFe-P-NAs [Figure 4F].

HYDROGEN EVOLUTION CORROSION

Hydrogen evolution corrosion is also a classic type of electrochemical corrosion reaction, driven spontaneously by the potential difference between species[30]. During this process, H^+ reacts with oxides and metals on the metal substrate surface, generating soluble metal ions that accumulate near the surface[53]. Since hydrogen evolution corrosion primarily leads to metal dissolution, it is difficult to grow corrosion products on the electrode material surface solely through hydrogen evolution corrosion. Therefore, in studies utilizing hydrogen evolution corrosion, the material surface is typically accompanied by other reactions[54], such as oxygen corrosion[55]. The purpose of these accompanying reactions is to capture metal ions near the electrode surface, thereby forming a stable, catalytically active layer on the surface.

Sun *et al.* synthesized amorphous (oxy)hydroxides with an optimal Fe/Ni atomic ratio as efficient OER electrocatalysts by combining hydrogen evolution corrosion and oxygen corrosion[56]. The iron-nickel foam (INF) is activated through immersion in 3 M HCl solution and subsequently undergoes growth in deionized water. During the activation process, H^+ reacts with the oxides and metals located on the metal substrate surface. The electrochemical potential difference between Fe (-0.44 V) and Ni (-0.257 V) within the INF facilitates the dissolution of the Fe component, thereby allowing for regulation of the Fe/Ni atomic ratio on the INF surface through controlled activation time (13-16)[30]. The growth process involves the oxidation of Fe^{2+} and the reduction of O_2 (15), leading to an increase in the pH of the metal surface and the formation of INF-S (16). INF-S exhibited enhanced electrocatalytic performance during the alkaline OER, achieving a low overpotential of 231 mV at a current density of 20 $mA·cm^{-2}$.

$$(Fe, Ni)O_x + 2xH^+ \rightarrow Fe^{2+} + Ni^{2+} + xH_2O \quad (13)$$

$$Fe + Ni + 4H^+ \rightarrow Fe^{2+} + Ni^{2+} + H_2\uparrow \quad (14)$$

$$4Fe^{2+} + O_2 + 2H_2O \rightarrow 4Fe^{3+} + 4OH^- \quad (15)$$

$$Fe^{3+} + Ni^{2+} + OH^- \rightarrow FeNi(oxy)hydroxides \quad (16)$$

The direct immersion of the metal substrate in an acid solution may cause excessive corrosion, which compromises the structural integrity of the substrate[57,58]. Zhou *et al.* developed an acidic gas corrosion strategy to prevent the metal substrate from contacting the solution, enabling the synthesis of a strongly coupled OER catalyst[59]. The method involved the delivery of dilute nitric acid to the nickel-IF surface through a vapor phase transport reaction (VPT) for corrosion, followed by ethanol immersion and combustion to synthesize the C-$NFF_{(5:5)}$-$LDH_{(6)}$/Fe_2O_3 catalyst [Figure 5A]. Transmission electron microscopy (TEM) characterization indicates that C-$NFF_{(5:5)}$-$LDH_{(6)}$/Fe_2O_3 exhibits a dense array of NiFe-LDH nanosheets, with Fe_2O_3 heterojunctions and abundant crystal-amorphous interfaces. The strong coupling between this structure and the metal substrate facilitates efficient electron transfer. *In situ* Raman shows that the presence of a proper amount of Fe triggers the structural reconstruction of C-$NFF_{(5:5)}$-$LDH_{(6)}$/Fe_2O_3 under alkaline electrooxidation conditions [Figure 5B], resulting in the formation of NiOOH and superoxide $NiOO^-$. C-$NFF_{(5:5)}$-$LDH_{(6)}$/Fe_2O_3 displayed outstanding OER performance, delivering a low overpotential of 220 mV at a current density of 10 $mA·cm^{-2}$, and remains stable for 100 h under 500 $mA·cm^{-2}$.

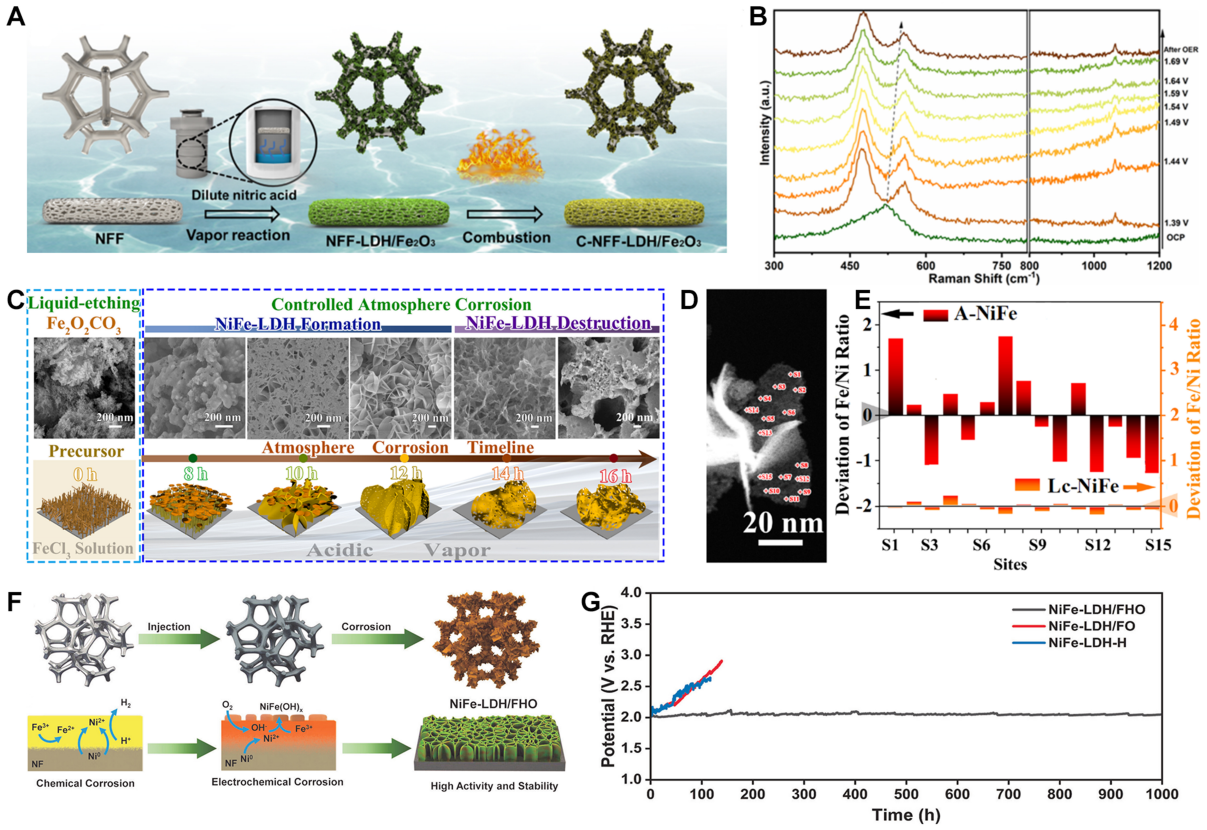

Figure 5. (A) Schematic of the synthesis for C-NFF$_{(x:y)}$-LDH$_{(t)}$/Fe_2O_3; (B) *In situ* Raman spectra of C-NFF$_{(5:5)}$-LDH$_{(6)}$/Fe_2O_3 at different potentials[59]. Reproduced under the terms of the Creative Commons Attribution License; (C) Morphology evolution and SEM mages of A-NiFe/NF electrode during the atmosphere corrosion process; (D) EDX probe locations on the STEM image of A-NiFe-LDH; (E) Point-by-point deviation of Ni/Fe atom-ratio on the A-NiFe and Lc-NiFe obtained from the EDX dot-analysis, zero represents the corresponding average value[60]. Reproduced under the terms of the Creative Commons Attribution License; (F) Synthesis diagram of NiFe-LDH macroporous array electrodes: (G) NiFe-LDH/FHO stability test at 500 mA·cm^{-2} for 1,000 h. Reproduced with permission[61]. Copyright 2023, Wiley-VCH. NFF: NiFe foam; LDH: layered double hydroxide; SEM: scanning electron microscope; NF: nickel foam; EDX: energy-dispersive X-ray spectroscopy; STEM: scanning transmission electron microscopy.

Furthermore, Du *et al.* employed an acidic gas corrosion strategy to fabricate A-NiFe/NF material with abundant edge/surface Fe defects on NF[60]. The Fe source was initially loaded onto the surface of the NF through liquid-phase corrosion. Subsequently, A-NiFe-LDH was generated in a sealed reactor via acid vapor corrosion [Figure 5C]. Imbalances in acid vapor permeation, coupled with ionization and limited mass transfer of localized Fe and Ni, cause an unequal stoichiometric ratio of Fe/Ni in the nanometer or subnanometer region [Figure 5D and E]. Benefiting from the abundant edge and surface Fe defects, A-NiFe-LDH showed outstanding OER performance. The overpotentials measured at 100 and 1,000 mA·cm^{-2} were 251 and 322 mV, respectively. It further sustained stable operation for 75 h at 100 mA·cm^{-2} without experiencing any degradation in performance. In addition, Song *et al.* successfully synthesized efficient catalytic materials using hydrogen evolution corrosion and oxygen corrosion[61]. An ethanol solution of iron nitrate and hydrochloric acid was injected into the pores of NF. After the evaporation of ethanol, Fe^{3+} and H^+ remained on the NF surface. NF experiences chemical corrosion via Fe^{3+} and H^+, leading to the dissolution of Ni^{2+}. In the electrochemical corrosion process with O_2, Ni^0 is oxidized to Ni^{2+}, while O_2 is reduced to form OH^-. NiFe-LDH/FHO with a macroporous array structure is successfully synthesized through the combination of $Fe^{2+}/^{3+}$ and Ni^{2+} with OH^- [Figure 5F]. The optimized NiFe-LDH/FHO electrode required only 180 and 248 mV to achieve 10 and 500 mA·cm^{-2} for the OER, respectively, and it exhibited

high stability for over 1,000 h at 500 mA·cm^{-2} [Figure 5G].

OXIDANT CORROSION

Oxidant corrosion is typically initiated by strong oxidizers such as H_2O_2, $S_2O_8^{2-}$, I_2, *etc.*[62-64]. These oxidizers react with the metal surface, accelerating dissolution and triggering substrate corrosion[65]. The variation in oxidant reduction products, local pH, and metal ion concentration promotes the formation of the target corrosion products. Compared to other types of corrosion, oxidant corrosion is faster and more damaging to facilitate the rapid synthesis of catalysts.

Recently, oxidant corrosion has been employed to synthesize a large number of electrocatalysts[62]. For example, Tu *et al.* employ the strong oxidizing capability of I_2 to oxidatively corrode NF, leading to the synthesis of I-NiS@NF[64]. The potential difference between I^{3-}/I^- (0.536 V) and Ni/Ni^{2+} (-0.257 V) facilitates the direct oxidation of Ni to Ni^{2+} by I_2. Meanwhile, the hydrolysis of $(NH_2)_2CS$ releases a significant amount of S^{2-}, providing a localized acidic environment that accelerates the corrosion of NF. In conclusion, fluffy NiS nanosheets are generated on the surface of NF as a result of the reaction between S^{2-} and Ni^{2+} released from thiourea hydrolysis. Additionally, Chen *et al.* establish a new method for the efficient and rapid synthesis of highly active self-supported Ni(Fe)OOH/Ni(Fe)S_x nanosheet arrays by leveraging fast corrosion with the oxidant $(NH_4)_2S_2O_8$ [Figure 6A][66]. NFF is corroded in a solution of $(NH_4)_2S_2O_8$, $(NH_2)_2CS$, and $FeCl_3$ to form defect-rich nanosheet arrays in only ten minutes. The heat released during the corrosion process significantly aids in the formation of OH^- and S^{2-} from the hydrolysis of $(NH_2)_2CS$, thereby expediting the growth of Ni(Fe)OOH/Ni(Fe)S_x. Experimental results show that Ni(Fe)S_x plays a vital role in improving OER performance. Ni(Fe)OOH/Ni(Fe)S_x demonstrates a lower overpotential in the OER compared to Ni(Fe)OOH, reaching current densities of 10 and 1,000 mA·cm^{-2} at overpotentials of 227 and 313 mV, respectively. Additionally, stable operation at 100 mA·cm^{-2} is maintained for a duration of 100 h.

Yu *et al.* synthesized a highly porous S-doped catalyst S-(Ni,Fe)OOH by immersing NF in a $Fe(NO_3)_3·9H_2O$ and $Na_2S_2O_3·5H_2O$ solution at room temperature for one to five minutes[67]. OH^- and S^{2-} are generated through the hydrolysis of $Na_2S_2O_3$, leading to the rapid binding of Ni^{2+} and Fe^{2+} with these species, resulting in the formation of S-(Ni,Fe)OOH. S-(Ni,Fe)OOH exhibited superior OER catalytic performance, attributed to its high density of active sites and the rapid release of bubbles. It necessitated overpotentials of only 300 and 398 mV to achieve current densities of 100 and 500 mA·cm^{-2}, respectively, in alkaline natural seawater. The electrolysis cell was constructed with S-(Ni,Fe)OOH as the anode and NiMoN as the cathode to assess the seawater electrolysis performance, achieving 500 mA·cm^{-2} with only 1.837 V in alkaline seawater. Simultaneously, stability testing at 500 mA·cm^{-2} for 100 h showed an increase in overpotential of just 70 mV.

Chen *et al.* synthesized large-area sulfidized stainless steel electrodes (MS/SS) through rapid interfacial reactions at room temperature[68]. Cations ($M^{\delta+}$, M = Fe, Ni, Cr) are released through the corrosion reaction of SS by Fe^{3+}, and these cations combine with S^{2-} formed from the hydrolysis of $S_2O_3^{2-}$ to produce metal sulfide (MS) [Figure 6B]. *In situ* Raman spectroscopic analysis suggests that MS/SS develops a highly active catalytic phase γ-(Ni,Fe)OOH in an alkaline environment [Figure 6C]. MS/SS is used as an anode in industrial alkaline electrolyzers. Furthermore, MS/SS achieves a catalytic current of approximately 300 mA·cm^{-2} under industrial conditions (30% KOH, 80 °C), maintaining good stability for over 120 h, demonstrating its potential for long-term operation in harsh electrochemical environments. Additionally, the same group synthesized bifunctional catalysts $(Ni,Fe)_3S_2$/NFF directly on large-area NFF surfaces by altering the metal substrate[69]. Successful synthesis of the heazlewoodite phase $(Ni,Fe)_3S_2$ on NFF is achieved by utilizing the oxidation of Fe^{3+} alongside the hydrolysis of sodium thiosulfate. Experimental characterization and theoretical calculations indicate that the Ni-Fe synergistic effect in $(Ni,Fe)_3S_2$ provides

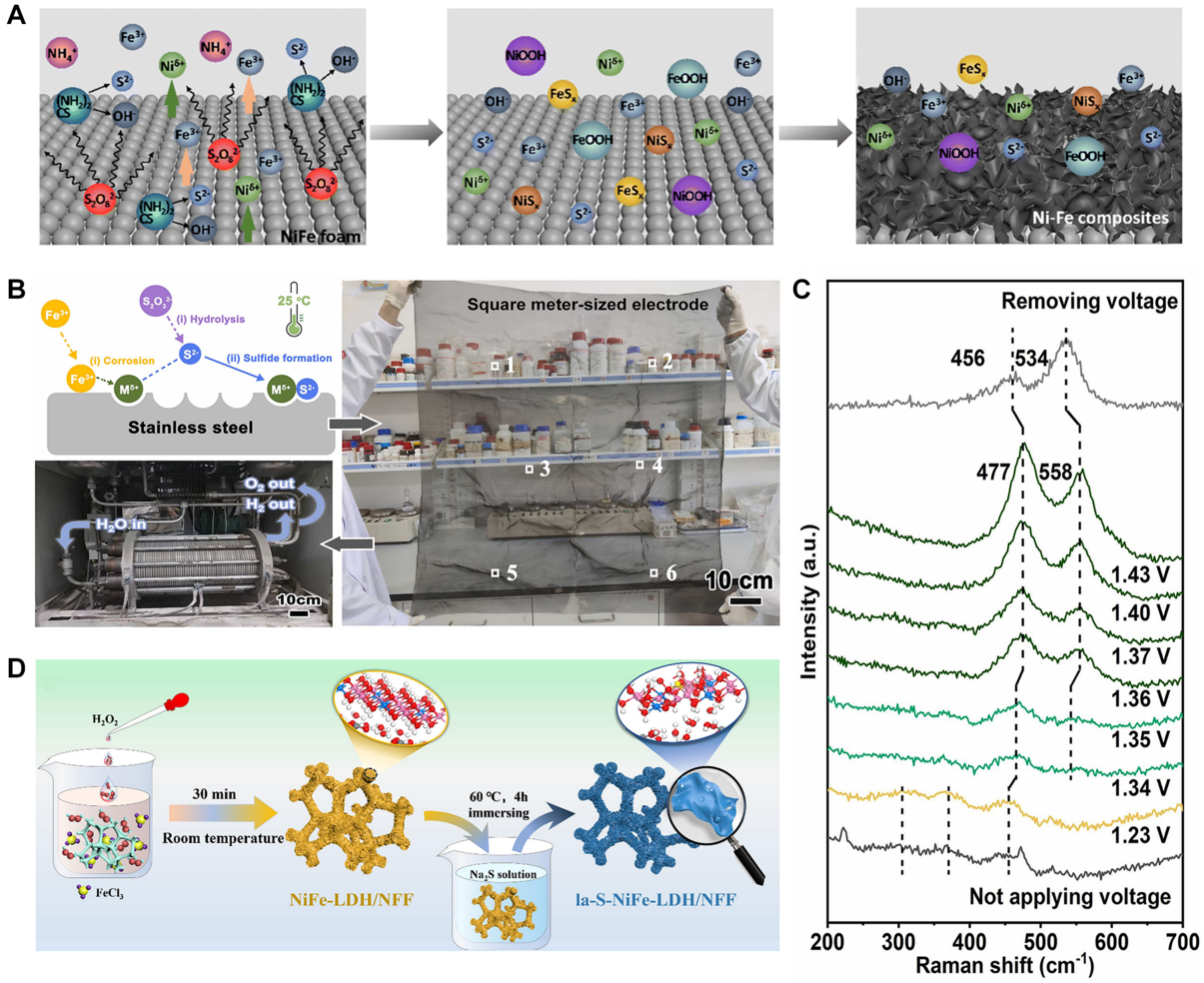

Figure 6. (A) Schematic of the preparation of Ni-Fe composite nanosheet array. Reproduced with permission[66]. Copyright 2023, Royal Society of Chemistry; (B) MS/SS forming schematic diagram, image of large area electrode (1 m × 1 m) and industrial alkaline electrolyzer photograph; (C) *In situ* Raman spectra of MS/SS during the OER at different voltages. Reproduced with permission[68]. Copyright 2022, Elsevier; (D) Scheme of synthesis process of la-S-NiFe-LDH/NFF. Reproduced with permission[71]. Copyright 2024, Elsevier. MS: Metal sulfide; SS: stainless steel; OER: oxygen evolution reaction; LDH: layered double hydroxide; NFF: NiFe foam.

high-density active sites for HER, such as Ni-Ni and Ni-Fe bridge sites. Concurrently, $(Ni,Fe)_3S_2$ nanosheets convert into the OER-active catalytic phase γ-(Ni,Fe)OOH during OER testing. It is shown that $(Ni,Fe)_3S_2$/NFF achieves a current density of 100 mA·cm^{-2} with overpotentials of only 241 mV for OER and 168 mV for HER. $(Ni,Fe)_3S_2$/NFF || $(Ni,Fe)_3S_2$/NFF shows remarkable catalytic performance (600 mA·cm^{-2} @ 1.93 V) and stability, operating reliably for more than 400 h at a high current density of 600 mA·cm^{-2}, which is better than the alkaline electrolyzer based on commercial Raney Ni electrodes.

Metal ions exhibit considerable advantages as oxidizing agents during corrosion[50]. They not only facilitate the dissolution of metals, but also enable the doping of metal elements into the material structure[70]. Lee *et al.* reported a one-step corrosion strategy for synthesizing dense $Ni_{0.75}Fe_{2.25}O_4$ NPs[38]. The process involves immersing NF in a Fe^{3+} hot solution for 36 h. This method relies on the distinct standard reduction potentials of Ni^{2+}/Ni (-0.25 V) and Fe^{3+}/Fe^{2+} (0.77 V) as the driving force. The rich grain boundaries and high-density NPs of $Ni_{0.75}Fe_{2.25}O_4$ result in lower charge transfer impedance and an increased number of active sites, thereby enhancing the OER activity. DFT calculations indicate that the Fe sites on the

$Ni_{0.75}Fe_{2.25}O_4$ NP surface are the main active sites, with partial substitution of Ni by Fe optimizing the occupation of the e_g orbitals and significantly improving OER performance. The $Ni_{0.75}Fe_{2.25}O_4$ NP electrode displays enhanced OER activity in 1 M KOH, reaching 10 mA·cm^{-2} at an overpotential of 192 mV, notably lower than the 265 mV needed by the commercial IrO_2 catalyst. The proton-exchange membrane (PEM) electrolyzer is constructed using $Ni_{0.75}Fe_{2.25}O_4$ NPs and Pt/C, realizing a water splitting current density of 2.0 A·cm^{-2} at a cell voltage of 1.9 V, which shows superior performance relative to electrolyzers employing IrO_2 and Pt/C catalyst combinations.

Utilizing oxidant corrosion can further alter the surface morphology, crystal structure, and electronic properties of the corrosion products[64]. Song *et al.* employ a two-step method involving H_2O_2 oxidative corrosion followed by anion modification to produce the la-S-NiFe-LDH/NFF [Figure 6D][71]. NFF is immersed in an H_2O_2-containing Fe^{3+} solution for 30 min, followed by anion exchange in a Na_2S solution. Fe^{3+} facilitates the formation of Fe^{2+} during the H_2O_2 oxidation process and triggers the Fenton reaction[72], which enhances the decomposition of H_2O_2 and the oxidation of metals. Meanwhile, the significant release of O_2 enhances the formation of basic hydroxides featuring larger interlayer spacing. During anion exchange, the NiFe-LDH nanosheets undergo reconstruction by S^{2-}. As immersion continues, NiFe-LDH/NFF transitions progressively from A crystalline to an amorphous state. Experimental characterizations and theoretical calculations indicate that S-induced local amorphous nanostructures strengthen the hybridization between Ni 3d and O 2p, enhancing metal–oxygen covalency and lattice oxygen activity, while reducing the O_2 desorption energy, thereby accelerating the OER process through the lattice oxygen mediated mechanism (LOM). As a result, the la-S-NiFe-LDH/NFF electrode demonstrated excellent OER catalytic performance, achieving low overpotentials of 245 and 252 mV at 100 mA·cm^{-2} in alkaline freshwater and seawater, respectively. Notably, the Pt/C || la-S-NiFe-LDH/NFF electrolyzer reached an industrial current density of 500 mA·cm^{-2} at a cell potential of 1.83 V for seawater electrolysis, maintaining stable operation for 100 h without significant degradation.

MICROBIAL CORROSION

Microbial corrosion is a method that utilizes the metabolic activities of specific microorganisms, such as Shewanella oneidensis MR-1[73] and anaerobic sulfate-reducing bacteria (SRB)[74], to induce the formation of beneficial corrosion products (e.g., nickel-iron hydroxides[75]) through the interaction between the metabolic products and metals or metal ions. This method integrates microbial corrosion with inorganic materials synthesis, facilitating the development of catalysts with enhanced OER performance under environmentally sustainable conditions[76].

Yang *et al.* reported an innovative application of microbial corrosion technology in the synthesis of nickel-iron hydroxides, successfully developing a highly efficient OER catalyst with a distinctive nanostructure[77]. Cleaned NF was submerged in reagent bottles containing different concentrations of anaerobic SRB [Figure 7A]. The SRB utilizes $^*H$ to reduce sulfate to sulfide, which subsequently interacts with dissolved Ni^{2+} to yield the bio-corrosion film Ni(Fe)$(OH)_2$-FeS_x [Figure 7B][78]. Experimental and theoretical investigations suggest that the high activity is attributed to the synergistic effect between Ni(Fe)OOH and Fe-S [Figure 7C]. The formation of $^*O$ on the Ni(Fe)OOH-FeS_x electrode is the rate-limiting step for OER. Incorporating Fe-S species strengthens the bonding between Fe and the active $^*O$ intermediate and significantly reduces the adsorption free energy gap. Ni(Fe)OOH-FeS_x achieves excellent electrochemical performance at reduced overpotentials, needing only 220 mV for a 10 mA·cm^{-2} current density and retaining good stability at 100 mA·cm^{-2} [Figure 7D].

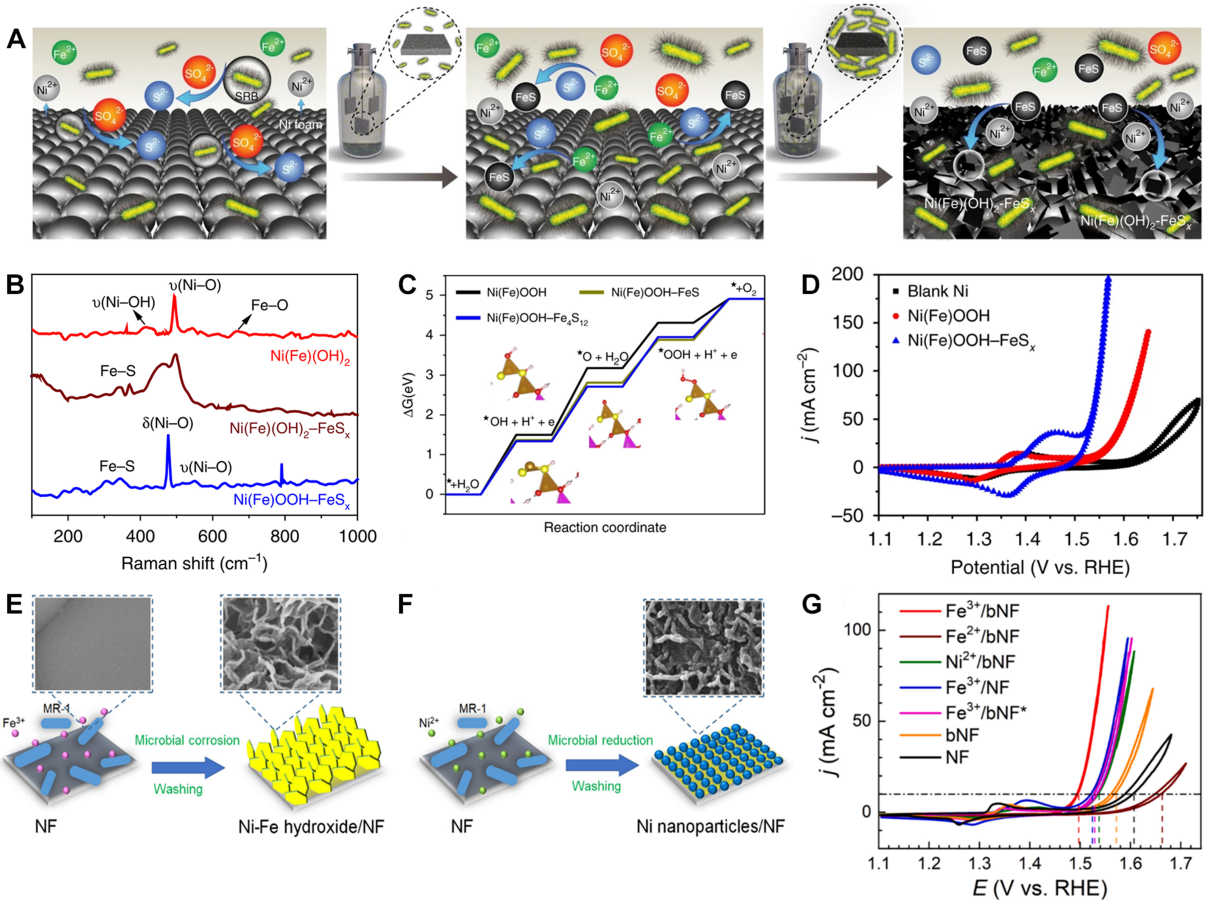

Figure 7. (A) Preparation diagram of Ni(Fe)$(OH)_2$-FeS_x electrode; (B) Raman spectra of corrosion-formed products; (C) Free energy diagram of corrosion-formed products; (D) CV profiles of different electrodes[77]. Reproduced under the terms of the Creative Commons Attribution License; (E) Microbial corrosion synthesis of Ni-Fe hydroxide/NF; (F) Microbial reduction synthesis of Ni NPs/NF; (G) Polarization curves of Fe^{3+}/bNF, Fe^{2+}/bNF, Ni^{2+}/bNF, Fe^{3+}/NF, Fe^{3+}/bNF*, bNF, and NF. Reproduced with permission[79]. Copyright 2024, Elsevier. CV: Cyclic voltammetry; NF: nickel foam; bNF: bio-treated nickel foam.

Microorganisms exhibit different corrosion behaviors in various solution environments due to the significant influence of environmental factors on their metabolism. Li *et al.* modify NF using the distinct corrosion behaviors exhibited by Shewanella oneidensis in various solution environments[79]. The NF and Shewanella oneidensis are enclosed in oxygen-free vials with different ionic solutions for five days, yielding a range of M/bNF catalysts. The research demonstrated that in Fe^{3+} solutions, Shewanella oneidensis accelerates NF corrosion, generating nanosheet structures of nickel iron hydroxides [Figure 7E]. In contrast, Shewanella oneidensis reduces nickel ions to synthesize nickel NPs in Ni^{2+} solutions [Figure 7F]. The modified Fe^{3+}/bNF catalyst exhibits significantly enhanced OER performance, requiring only a 0.265 V overpotential to achieve a current density of 10 mA·cm^{-2} [Figure 7G]. In addition, the utilization of an external magnetic field-assisted microbial corrosion strategy facilitates the development of novel and efficient oxygen evolution electrocatalysts. As reported by Zhang *et al.*, the introduction of an external magnetic field can expedite the corrosion processes of chemicals and SRB, promoting the production of FeS from SRB corrosion[75]. Theoretical investigations indicate that the integration of Ni(Fe)OOH into FeS promotes the optimization of O intermediate desorption from the NiOOH catalyst in the OER process, thereby lowering the energy barrier for the transformation from *O to *OOH. The synergistic effect between nickel iron hydroxide and FeS promotes the enhancement of OER activity. The synthesized Ni(Fe)$(OH)_2$-

FeS requires only a 287 mV overpotential to achieve a current density of 100 mA·cm^{-2}.

COST ESTIMATION FOR INDUSTRIAL PURPOSES

Cost plays a central role in the viability of a technology for widespread industrial adoption[80]. Considering our review on linking corrosion engineering with industrial applications, this section evaluates the costs associated with corrosion-synthesized materials to assess their potential for industrial application.

We begin with an electricity cost estimation. To enable a comparison across different electrode materials, we calculate the electricity cost for generating 1 m^3 of hydrogen in an alkaline electrolyzer under fixed conditions. At standard conditions (0 °C, 1 atm), 1 mol H_2 occupies roughly 22.4 L[81]. Thus, the molar quantity for 1 m^3 (1,000 L) of hydrogen is approximately 44.64 mol. Considering that the production of hydrogen is related to the amount of charge transferred, the total charge (Q) required to produce 44.64 mol of H_2 can be derived from Faraday's law, calculated by[82]:

$$Q = z \times n \times F = 2 \times 44.64 \text{ mol} \times 96485 \text{ C·mol}^{-1} = 8.61 \times 10^6 \text{ C} \quad (17)$$

Where n is the number of moles of the product, z is the number of electrons transferred by the product and F is the Faraday constant. Further, the electric energy consumed (W) at the operating voltage (U) of the electrolyzer can be determined, according to Joule's law, by[83]:

$$W = U \times I \times t = U \times Q = 2.393 \text{ U kW·h} \quad (18)$$

The actual operating voltage of the electrolyzer considers the theoretical electrolysis potential, overpotentials for both OER (η_{OER}) and HER (η_{HER}), and internal resistance losses (IR), which can be expressed as $U = 1.23 + \eta_{OER} + \eta_{HER} + IR$[84]. Since the electrode materials derived from corrosion engineering mainly exhibit excellent OER catalytic activity, for simplification, we assume that η_{HER} and IR are zero, meaning that the electricity cost based only on the theoretical electrolysis potential and η_{OER}. In other words, the estimated value we obtain represents the minimum electricity cost, and if we further consider the HER side, the associated electricity cost would increase further.

Based on the above analysis, we estimate the electricity cost associated with the electrode materials prepared via corrosion methods, as well as the alkaline commercial Raney nickel electrode, under a current density of 0.1 A·cm^{-2}, corresponding to the required operating voltage. These estimates, along with other relevant information, are summarized in Table 1. As shown, the power consumption of the corrosion-synthesized electrodes ranges from 3.4 to 3.7 kW·h under the above conditions, which is lower than the 4.0 kW·h for Raney nickel, indicating a performance advantage. Considering the current industrial electricity price ranging from 0.3 to 1.6 ¥/kW·h, the minimum threshold price of hydrogen, from the corrosion-prepared electrodes, can be estimated at 0.9 ¥/m^3 from the perspective of electricity cost.

The synthesis cost analysis for electrodes produced by corrosion methods and Raney nickel electrodes is also performed. The synthesis cost can be further broken down into raw material and equipment costs. The raw material prices mainly involved in the corrosion synthesis methods are presented, sourced from major reagent suppliers and Chinese manufacturers [Supplementary Table 1]. The primary cost of corrosion electrodes arises from the metal substrate and the raw materials used during processing. Due to the similarity in the processes of oxygen corrosion, hydrogen evolution corrosion and oxidant corrosion, their costs are almost equivalent. The complexity and high cost of the microbial cultivation process contribute to the higher overall cost for microbial corrosion. Therefore, the cost ranking is: microbial corrosion |||<***

Table 1. List of corrosion mechanism, corrosion product, corrosion speedup strategy, catalytic performance and cost estimation for catalysts synthesized based on corrosion engineering strategy

Corrosion mechanism	Catalyst	Substrate	Corrosion product	Corrosion speedup strategy	Current density @overpotential [mA·cm^{-2}@mV]	Electricity consumption for 1 m^3 H_2 [kW·h]	Ref.
Oxygen corrosion	3D-O_2-Cat-1	Fe foam	NiFe-LDH	-	$\eta_{100} \approx 220$ $\eta_{500} = 257$	3.5	[25]
Oxygen corrosion	NiFe-LDH@IF-200-72	Fe foam	NiFe-LDH	-	$\eta_{100} = 209$	3.4	[29]
Oxygen corrosion	$CoFe(OH)_x$-500/NFF	NFF	$CoFe(OH)_x$	Cl^-	$\eta_{100} = 274$	3.5	[37]
Oxygen corrosion	NF@NiFe-LDH-1.5-4	Ni foam	NiFe-LDH	Fe^{3+} Cl^-	$\eta_{100} = 190$	3.4	[43]
Oxygen corrosion	$NiFe_{1.833}(OH)_{0.5}O_{2.5}$	Stainless steel	$NiFe_{1.833}(OH)_{0.5}O_{2.5}$	T Cl^-	$\eta_{10} = 282$ $\eta_{100} \approx 410$	3.9	[47]
Oxygen corrosion	Pt-Co/Fe LDH	Fe foam	FeOOH, FeCo-LDH	H_2PtCl_6 Cl^-	$\eta_{100} = 285$	3.6	[51]
Oxygen corrosion	NiFe-O-NAs	Ni foam	Fe_2O_3, α-FeOOH	Cl^-	$\eta_{10} = 188$ $\eta_{100} \approx 255$ $\eta_{500} = 323$	3.5	[52]
Hydrogen evolution corrosion	INF-S	NFF	FeNi(oxy)hydroxides	-	$\eta_{10} \approx 243$ $\eta_{100} \approx 317$	3.7	[56]
Hydrogen evolution corrosion	C-$NFF_{(5:5)}$-$LDH_{(6)}$/Fe_2O_3	NFF	NiFe-LDH, Fe_2O_3	T	$\eta_{10} = 220$ $\eta_{100} \approx 385$	3.9	[59]
Hydrogen evolution corrosion	A-NiFe/NF	Ni foam	NiFe-LDH	Fe^{3+} Cl^-	$\eta_{100} = 251$ $\eta_{500} = 300$	3.5	[60]
Hydrogen evolution corrosion	NiFe-LDH/FHO	Ni foam	NiFe-LDH	T	$\eta_{10} = 180$ $\eta_{100} \approx 195$ $\eta_{500} = 248$	3.4	[61]
Oxidant corrosion	Ni(Fe)OOH/Ni(Fe)S_x	NFF	Ni(Fe)OOH, Ni_9S_8	$S_2O_8^{2-}$	$\eta_{10} = 227$ $\eta_{100} \approx 265$	3.4	[66]
Oxidant corrosion	MS/SS	Stainless steel	MS, M = Fe, Ni, Cr	Fe^{3+} $S_2O_3^{2-}$	$\eta_{100} \approx 300$	3.7	[68]
Oxidant corrosion	$(Ni, Fe)_3S_2$/NFF	NFF	$(Ni, Fe)_3S_2$	Fe^{3+} $S_2O_3^{2-}$	$\eta_{100} = 241$ $\eta_{500} \approx 350$	3.5	[69]
Oxidant corrosion	$Ni_{0.75}Fe_{2.25}O_4$ NPs	Ni foam	$Ni_{0.75}Fe_{2.25}O_4$	Fe^{3+} T	$\eta_{10} = 192$	-	[38]
Oxidant corrosion	Ia-S-NiFe-LDH/NFF	NFF	NiFe-LDH	H_2O_2	$\eta_{100} = 245$ $\eta_{500} = 283$	3.5	[71]
Microbial corrosion	Ni(Fe)$(OH)_2$-FeS_x	Ni foam	Ni(Fe)$(OH)_2$, FeS_x	Fe^{3+}	$\eta_{10} = 220$ $\eta_{100} \approx 315$	3.7	[77]
Microbial corrosion	Fe^{3+}/bNF	Ni foam	FeNi(oxy)hydroxides	Fe^{3+}	$\eta_{10} = 265$ $\eta_{100} \approx 307$	3.7	[79]

Microbial corrosion	$Ni(Fe)(OH)_2$-FeS	Ni foam	$Ni(Fe)(OH)_2$, FeS	Fe^{3+} magnetic	η_{100} = 287	3.6	[75]
-	Raney Ni	Ni mesh	-	-	$\eta_{100} \approx 432$	4.0	[85]

*T denotes the increase in the temperature of the reaction system. LDH: Layered double hydroxide; NFF: NiFe foam; NF: nickel foam; MS: metal sulfide; SS: stainless steel; NPs: nanoparticles.

oxygen corrosion ≈ hydrogen evolution corrosion ≈ oxidant corrosion.

The synthesis cost of a 0.25 m^2 circular electrode is estimated as a case study based on the industrial application scenario. The estimate is made solely based on our familiarity with the synthesis system and previous work[25]. Since the synthesis occurs spontaneously at ambient temperature, acrylic reaction vessels with acceptable corrosion resistance can be used, while ensuring that the volume of the corrosion solution is sufficient to cover the electrode material. Considering the custom cost of the acrylic container together with the price of the corrosion solution and the metal substrate, the total synthesis cost can be estimated to be around 1,200 ¥. Unlike corrosion-engineered electrodes, commercial Raney nickel requires plasma spraying equipment for its synthesis, which incurs higher processing costs, with a market value of approximately 1,500 ¥[86]. As demonstrated in the cost analysis, the corrosion method presents clear advantages over the Raney nickel electrodes. The scaling-up of corrosion-derived electrode materials for industrial purposes is both practically feasible and economically compelling.

CONCLUSION AND OUTLOOK

In this review, we systematically elaborate on various corrosion mechanisms, including oxygen corrosion, hydrogen evolution corrosion, oxidant corrosion, and microbial corrosion, and their applications in OER catalyst design. We also explore strategies to accelerate the corrosion process and modification methods of corrosion products, providing innovative perspectives and approaches for developing new high-efficiency catalysts. The results of related studies demonstrate that corrosion engineering shows great potential in preparing highly active and durable OER catalysts suitable for industrial applications. However, some challenges persist in fully applying corrosion engineering at an industrial production scale.

(1) Some fundamental reaction mechanisms in corrosion engineering remain unclear. The basic mechanisms are often inferred from the products and experimental phenomena, but there is a lack of *in-situ* characterizations to clarify the corrosion and growth mechanisms. Therefore, advanced *in-situ* characterization techniques, such as *in-situ* Raman, *in-situ* TEM, *in-situ* X-ray photoelectron spectroscopy (XPS), *etc.*, are needed to monitor the molecular structure and valence states of corrosion products, together with the solution composition of the corrosion reaction in real time. This would allow for precise identification of corrosion mechanisms and provide guidance for the preparation of electrocatalysts in corrosion engineering.

(2) To optimize corrosion methods for industrial applications, synthesis conditions should be chosen based on scalability, safety, and cost-effectiveness. The shift from small-scale lab production to large-scale industrial processes often leads to changes in the catalyst's microstructure and overall performance, making it challenging to maintain its activity and stability. As production scales up, the stability of raw material supply and cost-effectiveness become even more critical, highlighting the need for more affordable and accessible alternatives that can still yield high-performance catalysts. Furthermore, special attention must be given to evaluating whether the corrosion process can ensure the uniformity of large-scale electrodes meets the standards required for industrial production.

(3) Designing multi-component materials based on corrosion engineering. By innovating corrosion mechanisms, expanding the functionality and diversity of corrosion products is expected to promote the application of corrosion engineering in more fields. By exploring novel corrosion media and customizing corrosion environments, the dynamics and pathways of corrosion processes can be manipulated to create catalysts with unique compositions. Additionally, studying the corrosion behavior of active metals and rare earth metals can lead to corrosion products with distinctive electronic structures and surface properties during the corrosion process, which may exhibit excellent performance in catalytic applications.

(4) Developing special morphologies based on corrosion engineering, such as hierarchical nanostructured catalysts. Hierarchical nanostructures can significantly improve the surface hydrophilicity and gas repellency of the catalyst. At high current densities, these properties ensure rapid electrolyte coverage and efficient charge transfer, while also enabling quick bubble detachment. This would help maintain the catalyst's high activity and slow degradation, thus meeting the high current requirements of industrial applications.

(5) Broadening substrate types based on corrosion engineering. Currently, corrosion engineering primarily relies on iron, cobalt, nickel, and their alloys as metal substrates. However, when these corrosion-prone metals are used as catalyst supports, their structural stability still faces certain challenges. Therefore, developing effective methods for corroding other substrates, particularly for titanium mesh and some corrosion-resistant alloys, becomes especially important. Considering the application of seawater electrolysis, we are also exploring whether corrosion methods can be combined with seawater electrolysis. However, existing metal substrates that can undergo corrosion reactions face serious pitting corrosion in Cl^--rich seawater environments, leading to catalyst breakdown and deactivation. Finding substrates with higher Cl^--resistance that can function in seawater will be key to advancing the commercialization and scaling of seawater electrolysis.

DECLARATIONS

Authors' contributions

Manuscript preparation: Huang, Q., Liu, Y., Zhang, X.
Manuscript revision: Chen, H., Lin, S., Zou, X.

Availability of data and materials

Some results of supporting the study are presented in the Supplementary Materials. Further inquiries can be directed to the corresponding authors.

Financial support and sponsorship

This work was supported by the National Natural Science Foundation of China (No. 22279040 and No. 22369003), the Jilin Province Science and Technology Development Plan (No. 20240402080GH), the

Hainan Provincial Innovative Research Project of Postgraduates (Qhyb2023-173), Hainan Provincial Natural Science Foundation of China (Grant No. 223QN185) and Scientific Research Starting Foundation of Hainan University [Grant No. KYQD(ZR)-22022].

Conflicts of interest

Zou, X. is Section Editor of the journal *Chemical Synthesis*. Zou, X. was not involved in any steps of editorial processing, notably including reviewers' selection, manuscript handling and decision-making. The other authors declare that there are no conflicts of interest.

Ethical approval and consent to participate

Not applicable.

Consent for publication

Not applicable.

Copyright

REFERENCES

1. Ma, G.; Yang, N.; Xue, Y.; Zhou, G.; Wang, X. Ethylene glycol electrochemical reforming using ruthenium nanoparticle-decorated nickel phosphide ultrathin nanosheets. *ACS. Appl. Mater. Interfaces.* **2021**, *13*, 42763-72. DOI
2. Wang, M.; Feng, C.; Mi, W.; et al. Defect-induced electron redistribution between Pt-N_3S_1 single atomic sites and Pt clusters for synergistic electrocatalytic hydrogen production with ultra-high mass activity. *Adv. Funct. Mater.* **2024**, *34*, 2309474. DOI
3. Zhu, Y.; Chen, Y.; Feng, Y.; Meng, X.; Xia, J.; Zhang, G. Constructing Ru-O-TM bridge in NiFe-LDH enables high current hydrazine-assisted H_2 production. *Adv. Mater.* **2024**, *36*, e2401694. DOI
4. Li, Z.; Lin, G.; Wang, L.; et al. Seed-assisted formation of NiFe anode catalysts for anion exchange membrane water electrolysis at industrial-scale current density. *Nat. Catal.* **2024**, *7*, 944-52. DOI
5. Zeng, Y.; Zhang, X.; Ai, C.; Wang, C.; Liu, Y.; Lin, S. Orbital engineering of C_3N monolayer to design efficient synergistic sites electrocatalyst for boosting alkaline hydrogen evolution. *Appl. Surf. Sci.* **2022**, *582*, 152474. DOI
6. Tüysüz, H. Alkaline water electrolysis for green hydrogen production. *Acc. Chem. Res.* **2024**, *57*, 558-67. DOI PubMed PMC
7. Chade, D.; Berlouis, L.; Infield, D.; Cruden, A.; Nielsen, P. T.; Mathiesen, T. Evaluation of Raney nickel electrodes prepared by atmospheric plasma spraying for alkaline water electrolysers. *Int. J. Hydrogen. Energy.* **2013**, *38*, 14380-90. DOI
8. Ning, M.; Zhang, F.; Wu, L.; et al. Boosting efficient alkaline fresh water and seawater electrolysis *via* electrochemical reconstruction. *Energy. Environ. Sci.* **2022**, *15*, 3945-57. DOI
9. Wang, X.; Liu, X.; Wu, S.; et al. Phosphorus vacancies enriched cobalt phosphide embedded in nitrogen doped carbon matrix enabling seawater splitting at ampere-level current density. *Nano. Energy.* **2023**, *109*, 108292. DOI
10. Zhang, J.; Shang, X.; Ren, H.; et al. Modulation of inverse spinel Fe_3O_4 by phosphorus doping as an industrially promising electrocatalyst for hydrogen evolution. *Adv. Mater.* **2019**, *31*, e1905107. DOI
11. Zhang, X.; Jin, M.; Jia, F.; et al. Noble-metal-free oxygen evolution reaction electrocatalysts working at high current densities over 1000 mA cm^{-2}: from fundamental understanding to design principles. *Energy. Environ. Mater.* **2023**, *6*, e12457. DOI
12. Sun, H.; Xu, X.; Kim, H.; Jung, W.; Zhou, W.; Shao, Z. Electrochemical water splitting: bridging the gaps between fundamental research and industrial applications. *Energy. Environ. Mater.* **2023**, *6*, e12441. DOI
13. Li, X.; Han, S.; Qiao, Z.; Zeng, X.; Cao, D.; Chen, J. Ru monolayer island doped MoS_2 catalysts for efficient hydrogen evolution reaction. *Chem. Eng. J.* **2023**, *453*, 139803. DOI
14. Zhang, G.; Pei, J.; Wang, Y.; et al. Selective activation of lattice oxygen site through coordination engineering to boost the activity and stability of oxygen evolution reaction. *Angew. Chem. Int. Ed. Engl.* **2024**, *63*, e202407509. DOI
15. Shi, Z.; Zhang, X.; Lin, X.; et al. Phase-dependent growth of Pt on MoS_2 for highly efficient H_2 evolution. *Nature* **2023**, *621*, 300-5. DOI
16. Han, H.; Choi, H.; Mhin, S.; et al. Advantageous crystalline–amorphous phase boundary for enhanced electrochemical water oxidation. *Energy. Environ. Sci.* **2019**, *12*, 2443-54. DOI
17. Li, W.; Niu, Y.; Wu, X.; Wu, F.; Li, T.; Hu, W. Heterostructured $CoSe_2$/$FeSe_2$ nanoparticles with abundant vacancies and strong electronic coupling supported on carbon nanorods for oxygen evolution electrocatalysis. *ACS. Sustainable. Chem. Eng.* **2020**, *8*, 4658-66. DOI
18. Hu, M.; Qian, Y.; Yu, S.; et al. Amorphous MoS_2 decorated Ni_3S_2 with a core-shell structure of urchin-like on nickel-foam efficient hydrogen evolution in acidic and alkaline media. *Small* **2024**, *20*, e2305948. DOI

19. Shen, L.; Zhang, X.; He, H.; Fan, X.; Peng, W.; Li, Y. Template-assisted in situ synthesis of superaerophobic bimetallic MOF composites with tunable morphology for boosted oxygen evolution reaction. *J. Colloid. Interface. Sci.* **2024**, *676*, 238-48. DOI
20. Wang, N.; Song, S.; Wu, W.; Deng, Z.; Tang, C. Bridging laboratory electrocatalysts with industrially relevant alkaline water electrolyzers. *Adv. Energy. Mater.* **2024**, *14*, 2303451. DOI
21. Mehdi, M.; An, B.; Kim, H.; et al. Rational design of a stable Fe-rich Ni-Fe layered double hydroxide for the industrially relevant dynamic operation of alkaline water electrolyzers. *Adv. Energy. Mater.* **2023**, *13*, 2204403. DOI
22. Soo, J. Z.; Riaz, A.; Kremer, F.; et al. Cobalt modification of nickel–iron hydroxide electrocatalysts: a pathway to enhanced oxygen evolution reaction. *J. Mater. Chem. A.* **2023**, *11*, 22941-50. DOI
23. Sari, F. N. I.; Frenel, G.; Lee, A. C.; Huang, Y.; Su, Y.; Ting, J. Multi-high valence state metal doping in NiFe hydroxide toward superior oxygen evolution reaction activity. *J. Mater. Chem. A.* **2023**, *11*, 2985-95. DOI
24. Zhang, B.; Xiao, C.; Xie, S.; Liang, J.; Chen, X.; Tang, Y. Iron–nickel nitride nanostructures in situ grown on surface-redox-etching nickel foam: efficient and ultrasustainable electrocatalysts for overall water splitting. *Chem. Mater.* **2016**, *28*, 6934-41. DOI
25. Liu, Y.; Liang, X.; Gu, L.; et al. Corrosion engineering towards efficient oxygen evolution electrodes with stable catalytic activity for over 6000 hours. *Nat. Commun.* **2018**, *9*, 2609. DOI PubMed PMC
26. Lang, Z.; Song, G.; Wu, P.; Zheng, D. A corrosion-reconstructed and stabilized economical Fe-based catalyst for oxygen evolution. *Nano. Res.* **2023**, *16*, 2224-9. DOI
27. Ma, Y.; Wang, J.; Liu, H.; et al. Expediting corrosion engineering for sulfur-doped, self-supporting Ni-Fe layered dihydroxide in efficient aqueous oxygen evolution. *Catalysts* **2024**, *14*, 394. DOI
28. Jia, W.; Cao, X.; Chen, X.; et al. γ-MnO_2 as an electron reservoir for RuO_2 oxygen evolution catalyst in acidic media. *Small* **2024**, *20*, e2310464. DOI
29. Zhao, W.; Xu, H.; Luan, H.; et al. NiFe layered double hydroxides grown on a corrosion-cell cathode for oxygen evolution electrocatalysis. *Adv. Energy. Mater.* **2022**, *12*, 2102372. DOI
30. Liu, X.; Gong, M.; Deng, S.; et al. Transforming damage into benefit: corrosion engineering enabled electrocatalysts for water splitting. *Adv. Funct. Mater.* **2021**, *31*, 2009032. DOI
31. Kitiphatpiboon, N.; Chen, M.; Feng, C.; et al. Highly durable $FeNiS_x$/$NiFe(OH)_x$ electrocatalyst for selective oxygen evolution reaction in alkaline simulated seawater at high current densities. *Int. J. Hydrogen. Energy.* **2023**, *48*, 34255-71. DOI
32. Ke, C.; Zhao, Q.; Zhang, Y.; Yang, X.; Xiao, W. Corrosion-engineered stereoscopic nano-microflower FeOOH for efficient electrocatalysis toward oxygen evolution reaction. *J. Alloys. Compd.* **2023**, *955*, 170131. DOI
33. Liu, X.; Gong, M.; Xiao, D.; et al. Turning waste into treasure: regulating the oxygen corrosion on Fe foam for efficient electrocatalysis. *Small* **2020**, *16*, e2000663. DOI
34. Duan, S.; Liu, Z.; Zhuo, H.; et al. Hydrochloric acid corrosion induced bifunctional free-standing NiFe hydroxide nanosheets towards high-performance alkaline seawater splitting. *Nanoscale* **2020**, *12*, 21743-9. DOI
35. Li, Z.; Zhang, X.; Zhang, Z.; Chen, P.; Zhang, Y.; Dong, X. Dual-metal hydroxide@oxide heterojunction catalyst constructed via corrosion engineering for large-current oxygen evolution reaction. *Appl. Catal. B. Environ.* **2023**, *325*, 122311. DOI
36. Guo, X.; Zhang, F.; Evans, D. G.; Duan, X. Layered double hydroxide films: synthesis, properties and applications. *Chem. Commun.* **2010**, *46*, 5197-210. DOI
37. Wang, Y.; Zhuang, Y.; Yang, G.; Dong, C.; He, M. Unraveling the dynamic reconstruction of active Co(IV)-O sites on ultrathin amorphous cobalt-iron hydroxide nanosheets for efficient oxygen-evolving. *Small* **2024**, *20*, e2404205. DOI
38. Lee, J.; Jung, H.; Park, Y. S.; et al. Corrosion-engineered bimetallic oxide electrode as anode for high-efficiency anion exchange membrane water electrolyzer. *Chem. Eng. J.* **2021**, *420*, 127670. DOI
39. Zhang, Z. H.; Yu, Z. R.; Zhang, Y.; et al. Construction of desert rose flower-shaped NiFe LDH-Ni_3S_2 heterostructures *via* seawater corrosion engineering for efficient water-urea splitting and seawater utilization. *J. Mater. Chem. A.* **2023**, *11*, 19578-90. DOI
40. Liu, X.; Guo, X.; Gong, M.; et al. Regulated iron corrosion towards fabricating large-area self-supporting electrodes for an efficient oxygen evolution reaction. *J. Mater. Chem. A.* **2021**, *9*, 23188-98. DOI
41. Deng, J.; Wang, Z.; Yang, H.; et al. Superfast hydrous-molten salt erosion to fabricate large-size self-supported electrodes for industrial-level current OER. *Chem. Eng. J.* **2024**, *482*, 148887. DOI
42. Liu, S.; Ma, L.; Li, J. Facile preparation of amorphous NiFe hydroxide by corrosion engineering for electrocatalytic water and urea oxidation. *J. Alloys. Compd.* **2023**, *936*, 168271. DOI
43. Li, X.; Liu, C.; Fang, Z.; Xu, L.; Lu, C.; Hou, W. Ultrafast room-temperature synthesis of self-supported NiFe-layered double hydroxide as large-current-density oxygen evolution electrocatalyst. *Small* **2022**, *18*, e2104354. DOI
44. Xiao, Y.; Dastafkan, K.; Li, Y.; et al. Oxygen corrosion engineering of nonprecious ternary metal hydroxides toward oxygen evolution reaction. *ACS. Sustain. Chem. Eng.* **2022**, *10*, 8597-604. DOI
45. Liu, X.; Wang, X.; Gong, M.; Wang, R.; Hao, X.; Chen, Y. Corrosion strategy for synthesizing Ru-decorated FeOOH nanoneedles as advanced hydrogen evolution reaction catalysts. *J. Alloys. Compd.* **2023**, *958*, 170430. DOI
46. Gong, Z.; Wang, X.; Pi, W.; et al. Lattice contraction-driven design of highly efficient and stable O–NiFe layered double hydroxide electrocatalysts for water oxidation. *Mater. Today. Phys.* **2024**, *43*, 101399. DOI
47. Xia, J.; Zhang, J.; Huang, K.; et al. *In situ* growth of an active catalytic layer on commercial stainless steel *via* a hydrothermal-assisted corrosion process for efficient oxygen evolution reaction. *J. Mater. Chem. A.* **2024**, *12*, 19008-17. DOI
48. Zhang, Y.; Yang, C.; Zhao, L.; Zhang, J. Study on the electrochemical corrosion behavior of 304 stainless steel in chloride ion

solutions. *Int. J. Electrochem. Sci.* **2021**, *16*, 210251. DOI

49. Wu, Z.; Zhao, Y.; Wu, H.; et al. Corrosion engineering on iron foam toward efficiently electrocatalytic overall water splitting powered by sustainable energy. *Adv. Funct. Mater.* **2021**, *31*, 2010437. DOI
50. Zhao, Y.; Gao, Y.; Chen, Z.; et al. Trifle Pt coupled with NiFe hydroxide synthesized via corrosion engineering to boost the cleavage of water molecule for alkaline water-splitting. *Appl. Catal. B. Environ.* **2021**, *297*, 120395. DOI
51. Zhang, Z.; Zhang, Y.; Barras, A.; et al. Preparation of flower-shaped co-Fe layer double hydroxide nanosheets loaded with Pt nanoparticles by corrosion engineering for efficient electrocatalytic water splitting. *ACS. Appl. Energy. Mater.* **2022**, *5*, 15269-81. DOI
52. Zhang, X.; Zhu, H.; Zuo, Z.; et al. Robust and efficient Iron-Based electrodes for hydrogen production from seawater at high current density above 1000 mA cm^{-2}. *Chem. Eng. J.* **2024**, *490*, 151705. DOI
53. Guo, Y.; Xue, M.; Pan, Z.; Huo, X. L.; Bao, N.; Zhou, Q. Acid etching followed by water soaking: a top-down strategy to induce highly reactive substrates for electrocatalysis. *Chem. Commun.* **2023**, *59*, 3233-6. DOI
54. Haq, T. U.; Arooj, M.; Tahir, A.; Haik, Y. SO*x* functionalized NiOOH nanosheets embedded in $Ni(OH)_2$ microarray for high-efficiency seawater oxidation. *Small* **2024**, *20*, e2305694. DOI
55. Wang, P.; Lin, Y.; Xu, Q.; et al. Acid-corrosion-induced hollow-structured NiFe-layered double hydroxide electrocatalysts for efficient water oxidation. *ACS. Appl. Energy. Mater.* **2021**, *4*, 9022-31. DOI
56. Sun, C.; Song, Q.; Lei, J.; Li, D.; Li, L.; Pan, F. Corrosion of iron-nickel foam to in situ fabricate amorphous FeNi (Oxy)hydroxide nanosheets as highly efficient electrocatalysts for oxygen evolution reaction. *ACS. Appl. Energy. Mater.* **2021**, *4*, 8791-800. DOI
57. Yue, Y. Y.; Liu, C. J.; Shi, P. Y.; Jiang, M. F. Corrosion of hot-rolled 430 stainless steel in HCl-based solution. *Corros. Eng. Sci. Technol.* **2016**, *51*, 581-7. DOI
58. Fortes, J. C.; Terrones-Saeta, J. M.; Luís, A. T.; Santisteban, M.; Grande, J. A. Corrosion effect in carbon steel: process modeling using fuzzy logic tools. *Processes* **2023**, *11*, 2104. DOI
59. Zhou, Y.; Gao, J.; Ju, M.; et al. Combustion growth of NiFe layered double hydroxide for efficient and durable oxygen evolution reaction. *ACS. Appl. Mater. Interfaces.* **2024**, *16*, 28526-36. DOI
60. Du, S.; Ren, Z.; Wang, X.; Wu, J.; Meng, H.; Fu, H. Controlled atmosphere corrosion engineering toward inhomogeneous NiFe-LDH for energetic oxygen evolution. *ACS. Nano.* **2022**, *16*, 7794-803. DOI
61. Song, Y. F.; Zhang, Z. Y.; Tian, H.; Bian, L.; Bai, Y.; Wang, Z. L. Corrosion engineering towards NiFe-layered double hydroxide macroporous arrays with enhanced activity and stability for oxygen evolution reaction. *Chemistry* **2023**, *29*, e202301124. DOI
62. Yang, X.; Chen, Q.; Wang, C.; Hou, C.; Chen, Y. Substrate participation ultrafast synthesis of amorphous NiFe nanosheets on iron foam at room temperature toward highly efficient oxygen evolution reaction. *J. Energy. Chem.* **2019**, *35*, 197-203. DOI
63. Wang, J.; Teng, X.; Niu, Y.; et al. *In situ* autologous growth of self-supporting NiFe-based nanosheets on nickel foam as an efficient electrocatalyst for the oxygen evolution reaction. *RSC. Adv.* **2019**, *9*, 21679-84. DOI PubMed PMC
64. Tu, Z.; Liu, X.; Xiong, D.; et al. Ultrafast room-temperature activation of nickel foams as highly efficient electrocatalysts. *Chem. Eng. J.* **2023**, *475*, 146253. DOI
65. Ren, J. T.; Yuan, G. G.; Weng, C. C.; Chen, L.; Yuan, Z. Y. Uniquely integrated Fe-doped $Ni(OH)_2$ nanosheets for highly efficient oxygen and hydrogen evolution reactions. *Nanoscale* **2018**, *10*, 10620-8. DOI
66. Chen, M.; Li, W.; Lu, Y.; et al. Corrosion engineering approach to rapidly prepare Ni(Fe)OOH/Ni(Fe)S*x* nanosheet arrays for efficient water oxidation. *J. Mater. Chem. A.* **2023**, *11*, 4608-18. DOI
67. Yu, L.; Wu, L.; Mcelhenny, B.; et al. Ultrafast room-temperature synthesis of porous S-doped Ni/Fe (oxy)hydroxide electrodes for oxygen evolution catalysis in seawater splitting. *Energy. Environ. Sci.* **2020**, *13*, 3439-46. DOI
68. Chen, H.; Li, J.; Shen, Y.; et al. Room temperature, fast fabrication of square meter-sized oxygen evolution electrode toward industrial alkaline electrolyzer. *Appl. Catal. B. Environ.* **2022**, *316*, 121605. DOI
69. Bai, X.; Zhang, M.; Shen, Y.; et al. Room-temperature, meter-scale synthesis of heazlewoodite-based nanoarray electrodes for alkaline water electrolysis. *Adv. Funct. Mater.* **2024**, *34*, 2400979. DOI
70. Wang, L.; Ma, M.; Zhang, C.; et al. Manipulating the microenvironment of single atoms by switching support crystallinity for industrial hydrogen evolution. *Angew. Chem. Int. Ed. Engl.* **2024**, *63*, e202317220. DOI
71. Song, S.; Wang, Y.; Tian, P.; Zang, J. Activating lattice oxygen in local amorphous S-modified NiFe-LDH ultrathin nanosheets toward superior alkaline/natural seawater oxygen evolution. *J. Colloid. Interface. Sci.* **2025**, *677*, 853-62. DOI
72. Qi, J.; Jiang, G.; Wan, Y.; Liu, J.; Pi, F. Nanomaterials-modulated Fenton reactions: Strategies, chemodynamic therapy and future trends. *Chem. Eng. J.* **2023**, *466*, 142960. DOI
73. Jia, S.; Shen, Q.; Yong, Y.; Mi, J. *In situ* modification of metal electrode by integrated microbial corrosion and microbial mineralization using *Shewanella oneidensis* for efficient oxygen evolution. *Catal. Sci. Technol.* **2023**, *13*, 2447-57. DOI
74. Yang, H.; Dong, C.; Wang, H.; et al. Constructing nickel-iron oxyhydroxides integrated with iron oxides by microorganism corrosion for oxygen evolution. *Proc. Natl. Acad. Sci. U. S. A.* **2022**, *119*, e2202812119. DOI PubMed PMC
75. Zhang, X.; Chen, Y.; Ye, Z.; et al. Magnetic field-assisted microbial corrosion construction iron sulfides incorporated nickel-iron hydroxide towards efficient oxygen evolution. *Chin. J. Struct. Chem.* **2024**, *43*, 100200. DOI
76. Zhang, W.; Ying, J.; Liu, H. Biomineralization of sulfate-reducing bacteria in situ-induced preparation of nano Fe_2O_3-Fe(Ni)S/C as high-efficiency oxygen evolution electrocatalyst. *Small* **2024**, *20*, e2307808. DOI
77. Yang, H.; Gong, L.; Wang, H.; et al. Preparation of nickel-iron hydroxides by microorganism corrosion for efficient oxygen evolution.

Nat. Commun. **2020**, *11*, 5075. DOI PubMed PMC
78. Zhang, W.; Liu, H.; Ying, J.; Liu, H. Preparation of nickel–iron sulfide/oxide nanocomposites by biomineralization of sulfate-reducing bacterium for efficient oxygen evolution. *Chem. Eng. J.* **2023**, *475*, 146211. DOI
79. Li, J.; Mi, J.; Qing, Z.; et al. In-situ modification of nickel electrode by coupling the microbial corrosion and microbial reduction using Shewanella oneidensis for enhanced electrocatalysis. *Chem. Eng. J.* **2024**, *495*, 153176. DOI
80. Meharban, F.; Lin, C.; Wu, X.; et al. Scaling up stability: navigating from lab insights to robust oxygen evolution electrocatalysts for industrial water electrolysis. *Adv. Energy. Mater.* **2024**, *14*, 2402886. DOI
81. Wang, M.; Sun, X.; Janssen, P.; Tang, S.; Tan, Z. Responses of methane production and fermentation pathways to the increased dissolved hydrogen concentration generated by eight substrates in in vitro ruminal cultures. *Anim. Feed. Sci. Technol.* **2014**, *194*, 1-11. DOI
82. Zhao, S.; Wang, S.; Qiu, C.; et al. Enhanced electrocatalytic alcohol oxidation mediated with ultra-low concentration of aminoxyl radicals via an Intermediate-Rich local microenvironment. *Chem. Eng. Sci.* **2024**, *286*, 119653. DOI
83. Xiao, A.; Ban, F.; Tong, X.; Ye, C.; Wei, Y. Electrochemical treatment of azo dye wastewater by dynamic flow diaphragm system: response surface methodology optimization and energy consumption analysis. *Desalination. Water. Treat.* **2024**, *320*, 100615. DOI
84. Zhang, K.; Liang, X.; Wang, L.; et al. Status and perspectives of key materials for PEM electrolyzer. *Nano. Res. Energy.* **2022**, *1*, e9120032. DOI
85. Li, T.; Liu, W.; Xin, H.; et al. Large-scale and simple synthesis of $NiFe(OH)_x$ electrode derived from raney Ni precursor for efficient alkaline water electrolyzer. *Catalysts* **2024**, *14*, 296. DOI
86. Zhu, Z.; Lin, Y.; Fang, P.; et al. Orderly nanodendritic nickel substitute for raney nickel catalyst improving alkali water electrolyzer. *Adv. Mater.* **2024**, *36*, e2307035. DOI

Quanbin Huang

Quanbin Huang obtained a bachelor's degree from Hainan University in 2023. His primary research focuses on OER and HER catalytic materials for hydrogen production through water electrolysis.

Xu Zhang

Xu Zhang is currently pursuing a doctoral degree at Hainan University. His research centers on the development and application of efficient materials for water electrolysis.

Shiwei Lin

Shiwei Lin is a Professor in the School of Materials Science and Engineering at Hainan University, China. He received his PhD from the University of Manchester in 2006 and obtained his B.Eng. and M.Eng. degrees in Materials Science and Engineering from Tsinghua University (1996-2002). He has been with Hainan University since 2007. His research interests include the rational design and structure modification of photoelectrochemical materials and devices, chemical sensors, and computational materials science.

Yipu Liu

Yipu Liu obtained her Ph.D. from Jilin University in 2019. She is currently an Associate Professor at Hainan University. Her research focuses on the theoretical prediction and synthesis of functional materials for catalysis reactions (HER, OER, ORR, *etc.*).

Xiaoxin Zou

Xiaoxin Zou obtained his Ph.D. in inorganic chemistry from Jilin University (China) in June 2011. He subsequently worked as a postdoctoral scholar at the University of California, Riverside, and Rutgers, The State University of New Jersey, from July 2011 to October 2013. He is now a Professor at the State Key Laboratory of Inorganic Synthesis and Preparative Chemistry, Jilin University. His research interests include hydrogen energy materials chemistry, with a focus on elucidating the atomic basis of water-splitting electrocatalysts, predicting and discovering efficient catalysts with novel crystal structures, and developing preparative technologies for industrial water-splitting catalysts.

Hui Chen

Hui Chen earned his Ph.D. in materials science from Jilin University (China) in June 2018 and completed his postdoctoral training at the College of Chemistry, Jilin University, from June 2018 to November 2022. He is currently a Professor at the State Key Laboratory of Inorganic Synthesis and Preparative Chemistry, Jilin University. His research specializes in catalytic materials for water electrolysis technologies, including alkaline water electrolyzer (AWE) and proton exchange membrane water electrolyzer (PEMWE). Recent advancements in his work include (i) the development of low-iridium oxygen-evolution catalysts and anode catalyst layers for PEMWEs and (ii) the large-area synthesis of highly active and stable nickel-based electrodes for AWEs. He has authored 40+ peer-reviewed papers and 10 patents. In 2024, he joined the editorial board of *Chemical Synthesis*.